SURFACE ROUGHNESS SCATTERING OF ELECTRONS IN BULK MOSFETS

BY

AMANDA ZUVERINK

THESIS

A project report submitted in partial fulfillment of the requirements for the degree of

Master of Science

(Electrical Engineering)

at the

UNIVERSITY OF WISCONSIN-MADISON

2015

Abstract

Surface-roughness scattering of electrons at the Si-SiO_2 interface is a very important consideration when analyzing Si metal-oxide-semiconductor field-effect transistors (MOSFETs). Scattering reduces the mobility of the electrons and degrades the device performance. 250-nm and 50-nm bulk MOSFETs were simulated with varying device parameters and mesh sizes in order to compare the effects of surface-roughness scattering in multiple devices. The simulation framework includes the ensemble Monte Carlo method used to solve the Boltzmann transport equation coupled with a successive over-relaxation method used to solve the two-dimensional Poisson's equation. Four methods for simulating the surface-roughness scattering of electrons were implemented on both devices and compared: the constant specularity parameter, the momentum-dependent specularity parameter, and the real-space-roughness method with both uniform and varying electric fields. The specularity parameter is the probability of an electron scattering specularly from a rough surface. It can be chosen as a constant, characterizing partially diffuse scattering of all electrons from the surface the same way, or it can be momentum dependent, where the size of rms roughness and the normal component of the electron wave number determine the probability of electron-momentum randomization. The real-space rough surface method uses the rms roughness height and correlation length of an actual MOSFET to simulate a rough interface. Due to their charge, electrons scatter from the electric field and not directly from the surface. If the electric field is kept uniform, the electrons do not perceive the roughness and scatter as if from a flat surface. However, if the field is allowed to vary, the electrons scatter from the varying electric field as they would in a MOSFET. These methods were implemented for both the 50-nm and 250-nm MOSFETs, and using the rms roughness heights and correlation lengths for real devices. The current–voltage and mobility–electric field curves were plotted for each method on the two devices and compared. The conclusion is that the specularity-parameter methods are valuable as simple models for relatively smooth interfaces. However, they have limitations, as they cannot accurately describe the drastic reduction in the current and the electron mobility that occur in MOSFETs with very rough Si-SiO_2 interfaces.

Acknowledgments

This thesis would not be possible without the aid and support of numerous people. First, I would like to thank my advisor, Irena Knezivic, for all her supervision and guidance throughout the course of this project. I would also like to thank the nanoelectronics theory group, especially Leon Mauer, Song Mei, and Amirhossein Davoody for their invaluable assistance, advice, and devoted time. With much gratitude, I would like to thank my manager, Robert Mata at Sandia National Laboratories, for believing in me. I consider it a great honor to have received The Master's Fellowship Award which funded this project and allowed me to fully focus on completing my masters degree. Finally, I would like to thank my parents and my amazing husband, Mark Zuverink, for their utmost love, support, and encouragement.

Contents

List of Figures

List of Tables

1 Introduction

1.1 Surface-Roughness Scattering

Electron transport through metal-oxide-semiconductor field-effect transistor (MOSFET) devices is affected by various scattering mechanisms which shorten the free flight of the electrons flowing inside the device [1–4]. Electrons scattering can reduce the electron channel mobility [1] and decrease the amount of current that is able to flow through the device [4]. These effects are particularly noticeable when the device is operating at lower temperatures [1]. Although there are many scattering mechanisms within the device that can act upon the electrons, certain scattering mechanisms dominate throughout different regions of the device depending on the probability of each specific scattering mechanism; if more than one scattering mechanism is active, the type with the largest probability takes precedence [2–4].

The boundary between silicon (Si) and silicon dioxide (SiO_2) interface at the surface of the device is rough [1–4] and, since electrons are not allowed to enter the oxide, they must scatter from the rough surface [3]. The surface roughness at the Si-SiO_2 interface occurs during the oxide growth stage of fabrication [2]. The roughness of this boundary is affected by the temperature during the oxide growth and the temperature during the post-oxidation annealing phase [4]. The roughness at the Si-SiO_2 interface leaves a fluctuation of thickness in the oxide, as well as an inconsistent minimum boundary at the surface in the channel region of the device [2], which causes the electric field to vary at the Si-SiO_2 interface [5]. The variation in the electric field causes the electron to scatter [1–5]. Since most electrons are located within the channel region of the device during inversion, the surface-roughness scattering becomes a dominating scattering mechanism in the channel region of the device, particularly with a larger rms roughness height or with a higher electron concentration [1–3]. For an unintentionally roughened interface between Si and SiO_2 the rms roughness height is measured to be on the order of 2 Å, as measured using cross-sectional high-resolution transmission electron microscopy (HRTEM) [1]. The rms roughness height for an unintentionally roughened interface is relatively low and looks almost smooth with only a few steps into the Si surface, as shown in Figure 1(a) [1]. The rms roughness height for an intentionally roughened surface was measured to be approximately 3 Å [1], however, even though the rms roughness height did not change much, the roughness is more apparent, as seen in Figure 1(b), which causes an increased level of scattering.

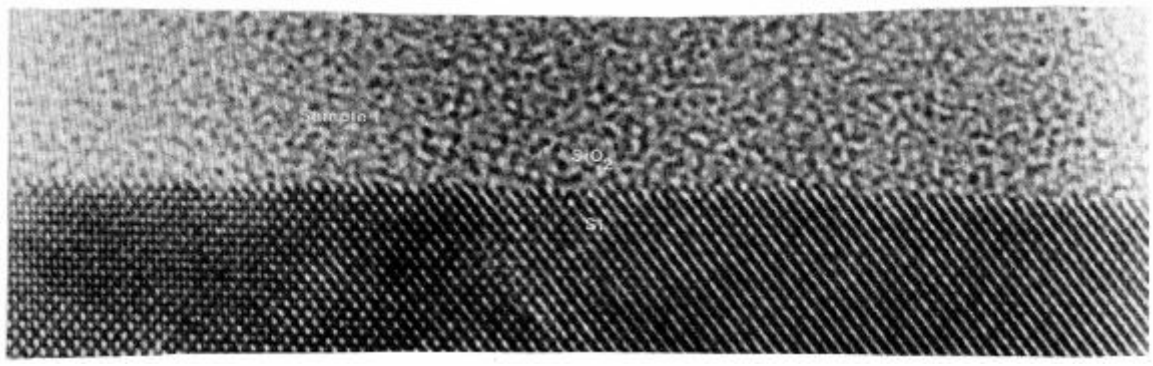

(a)

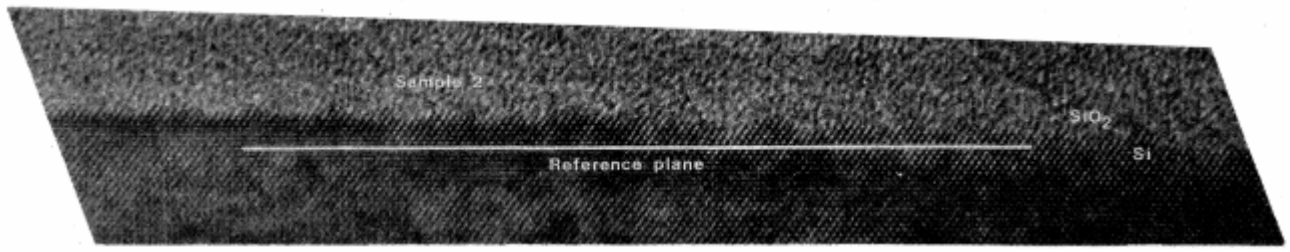

(b)

Figure 1: High-magnification pictures of an (a) unintentionally roughened and an (b) intentionally roughened Si-SiO_2 interface in a Si(100) MOSFETs taken using cross-sectional high-resolution transmission electron microscopy. (From Goodnick *et al.* [1])

This report will focus on the surface-roughness scattering at the Si-SiO_2 interface in a planar bulk MOSFET devices [3, 4]. First, the basic description of the bulk MOSFET devices will be explained, followed by an explanation of the device simulation framework used to model the MOSFET devices. Second, we will explain the four different ways in which surface roughness was modeled: constant spectularity parameter, momentum-dependent specularity parameter, and real-space roughness with and without a varying electric field. Lastly, the results of the simulations for each of the different approaches of modeling surface-roughness scattering in both MOSFET devices are displayed and compared to show the accuracy and real-world validity for each of the different methods.

1.2 MOSFET Description

A MOSFET is a planar four-terminal semiconducting device with source, drain, gate, and substrate terminals [3]. MOSFETs are fabricated with Si due to its abundance and the easy growth of SiO_2 on top of Si [3,4]. MOSFETs can be n-type (majority carriers are electrons) or p-type (majority carriers are holes.) For the purposes of this paper the focus will be on n-type MOSFETs, such as the one shown in Figure 2 [3]. Electrons move from the source terminal of the device, which is generally grounded, to the drain terminal of the device through the n-type channel. The channel is induced by a positive voltage being applied to the gate terminal of the device [3], which lowers the potential barrier, allowing

electrons to flow [4]. The larger the voltage applied to the gate, the larger the current through the device, since more electrons are able to flow from the source to the drain due to the lower potential barrier [4]. The fourth terminal of the device is the substrate, which is attached to the p-type substrate of the device and is usually grounded [3]. The MOSFETs that were simulated are two-dimensional MOSFETs with a 250 nm channel length and a 50 nm channel length, and with device dimensions of Table 1 and doping concentrations of Table 2.

MOSFET Device Dimensions					
Channel Length	Source/Drain Length	Source/Drain Depth	Bulk Depth	Device Width	Oxide Thickness
250 nm	50 nm	36 nm	400 nm	1.4 μm	5 nm
50 nm	22.5 nm	10 nm	120 nm	7.3 μm	1.5 nm

Table 1: Device dimensions for the 50-nm and 250-nm MOSFETs.

MOSFET Doping Concentrations		
Channel Length	Source/Drain Doping Concentration	Bulk Doping Concentration
250 nm	10^{19} cm^{-3}	10^{16} cm^{-3}
50 nm	$2{\cdot}10^{19}$ cm^{-3}	10^{15} cm^{-3}

Table 2: Doping concentrations for the 50-nm and 250-nm MOSFETs.

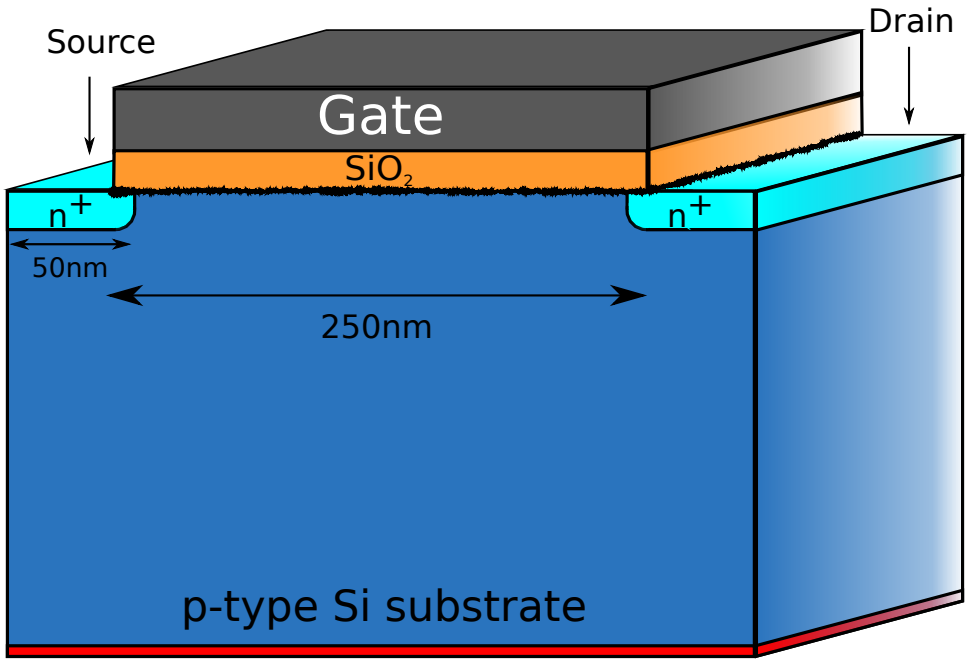

Figure 2: A three-dimensional schematic of an n-type MOSFET with 50 nm source and drain terminals, a 250 nm channel length, and roughness shown at the Si-SiO_2 interface.

2 Device Simulation

The MOSFET simulator uses the device parameters from section 1.2 in order to create a two-dimensional mesh of the device. Using these parameters a starting number of electrons are initialized and placed into the mesh cells. When the device is still in equilibrium, the potential, electric field, and electron distribution are calculated for each mesh cell. Voltage is then applied to the gate and drain terminals, and the electrons are allowed to move along the channel. The motion of electrons occurs for a time step where each electron is tracked as it moves from one mesh cell to another. Each electron keeps a constant direction and magnitude until it scatters via one of the simulated mechanisms (surface-roughness scattering, acoustic scattering, intervalley scattering, Coulomb scattering, and boundary scattering), and then a new direction and magnitude is calculated accordingly. If the electron reaches the source/drain, the electron exits the device and eliminated. New electrons are also created and enter the device via the source/drain. Once the motion of electrons is simulated, the new potential, electric field, and electron distribution is determined. At the end of the time step the electrons entering/exiting the device is sampled, and a new time step begins. The time step iterations continue until the device reaches steady state.

2.1 Ensemble Monte Carlo Method

Electron transport through a MOSFET device can be described by the Boltzmann transport equation (BTE). The BTE is the continuity equation for the flow of particles in the six-dimensional phase space of both position and momentum. Given in its common form, the BTE is [4, 14]:

$$\frac{\partial f}{\partial t} + \vec{\mathrm{v}} \cdot \nabla_{\vec{r}} f + \hbar \frac{d\vec{k}}{dt} \cdot \nabla_{\vec{k}} f = \sum_{\vec{k}'} \{ S(\vec{k}', \vec{k}) f(\vec{k}') [1 - f(\vec{k})] - S(\vec{k}, \vec{k}') f(\vec{k}) [1 - f(\vec{k}')] \}, \quad (1)$$

where $f(\vec{r}, \vec{k}, t)$ is the one-particle distribution function which gives the probability of finding an electron within $d^3\vec{r}$ of position $\vec{r}$ and within $d^3\vec{k}$ of wavevector $\vec{k}$ at time t. Where $\hbar$ is Planck's constant, $\vec{\mathrm{v}}$ is the particle's velocity, and the right-hand side of the equation is the collision integral, which is the net scattering of the electrons from the different in and out scattering mechanisms $S(\vec{k}', \vec{k})$ represents the transition rate from the initial state $(\vec{k})$ to the final state $(\vec{k}')$ [4, 14]. The BTE describes a semiclassical approach to describing the transport of electrons inside of a device, since it treats particles as if they have an explicit position and momentum (which violates Heisenberg's uncertainty principle); however, the dynamics and scattering processes of the particles are treated quantum mechanically [4, 14].

The ensemble Monte Carlo (EMC) technique is a numerical method to directly solve

the BTE [4, 15]. The basic process of the EMC technique is to simulate the motion of a particle during a set time step for each particle Δt, where the particle will experience free flight and collisions with other particles (such as phonons and impurities) which causes the particle to scatter. This process of free flights and scattering events for each particle occurs until the time step is complete, as shown in Figure 3 [4, 15, 16]. Scattering events are treated as instantaneous [14]. Additionally, the duration of the free flight and scattering mechanisms of the particles are selected stochastically according to given probabilities describing the process, which relies on generated random numbers [4, 15]. These random numbers are also used to determine which scattering mechanism terminated the free flight of the particles, as well as to determine the new wavevector [14]. The EMC process continues for each electron until the simulation reaches steady state. The motion at various times of the simulation may be sampled in order to estimate the value of interesting quantities such as the average energy, the average drift velocity in the presence of an electric field, and the average current, where these terms are averaged across the depth of the MOSFET [4, 14].

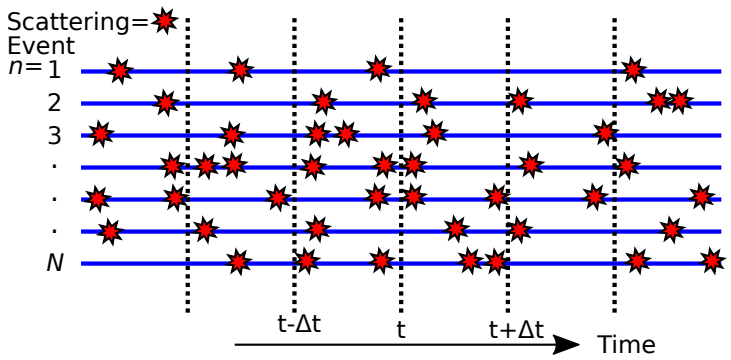

Figure 3: Flight Dynamics schematic for Ensemble Monte Carlo simulation. The horizontal lines display the trajectories that particles 1-N take through time. The dotted vertical lines represent the sampling times separated by Δt, and the stars represent the scattering events

During the free flight of the electron in the MOSFET simulation shown in Figure 4, the electron drifts a small amount in the x and y directions and the boundaries of the device are checked in order to determine if the electron scattered from a boundary in order to keep the electron inside the device. If the electron hits the top of the source or drain of the device then the electron scatters outside of the device and is deleted. At some point in the free flight the electron scatters from another particle and a single scattering mechanism is chosen. In the MOSFET simulation, the scattering mechanisms that an electron could scatter from are acoustic (phonon), intervalley (phonon), and Coulomb (impurity) scattering mechanisms, as well as the self-scattering mechanism which is used to maintain a constant total scattering rate [4]. Once the scattering mechanism is chosen, the energies and wavevectors are updated according to the chosen scattering mechanism

and the energy and momentum conservation laws respectively [4, 14]. The electron then continues to drift and the process continues until the time step is finished. Afterward, extra electrons are eliminated and new electrons are created at the source and drain contacts.

Since the charges used in the free flight part of the EMC are distributed within the mesh cells instead of being located at discrete grid points inside the device, the particle mesh method (PM) is used in order to move the charge from the mesh cell to discrete grid points at the corners of the cell [17]. The PM method that is used is the nearest-element-center (NEC) scheme. The NEC scheme was chosen because it reduces the self-forces and increases the spatial accuracy. The NEC PM method is carried out in four steps. First, the charges are assigned to the mesh by dividing the charges in the cell equally into four corner grid points originally surrounding the charge [4]. Then the two-dimensional nonequilibrium Poisson's equation is solved at these grid points using the SOR method as described in detail in section 2.2 [4, 17]. Afterward the electric fields are calculated from these points from using the new potential calculated from the two-dimensional Poisson's equation and lastly the field is interpolated in order to find the force on each charge [4] [17]:

$$E^x_{i,j} = \frac{(\phi_{i,j} - \phi_{i+1,j})}{dx}, \qquad E^y_{i,j} = \frac{(\phi_{i,j} - \phi_{i,j+1})}{dy}, \tag{2}$$

where dx and dy are spacing between the mesh grid points, which is the mesh size, and $E^x_{i,j}$ and $E^y_{i,j}$ are the electric fields in the lateral and transverse directions respectively [4]. Then, the motion of the electrons is sampled in order to calculate the average energy, average drift velocity, and average current [4]. Lastly, the net number of electrons entering and exiting the source and the drain contacts during the EMC simulation are calculated in order to calculate the current, as described in more detail in section 4.1 [4].

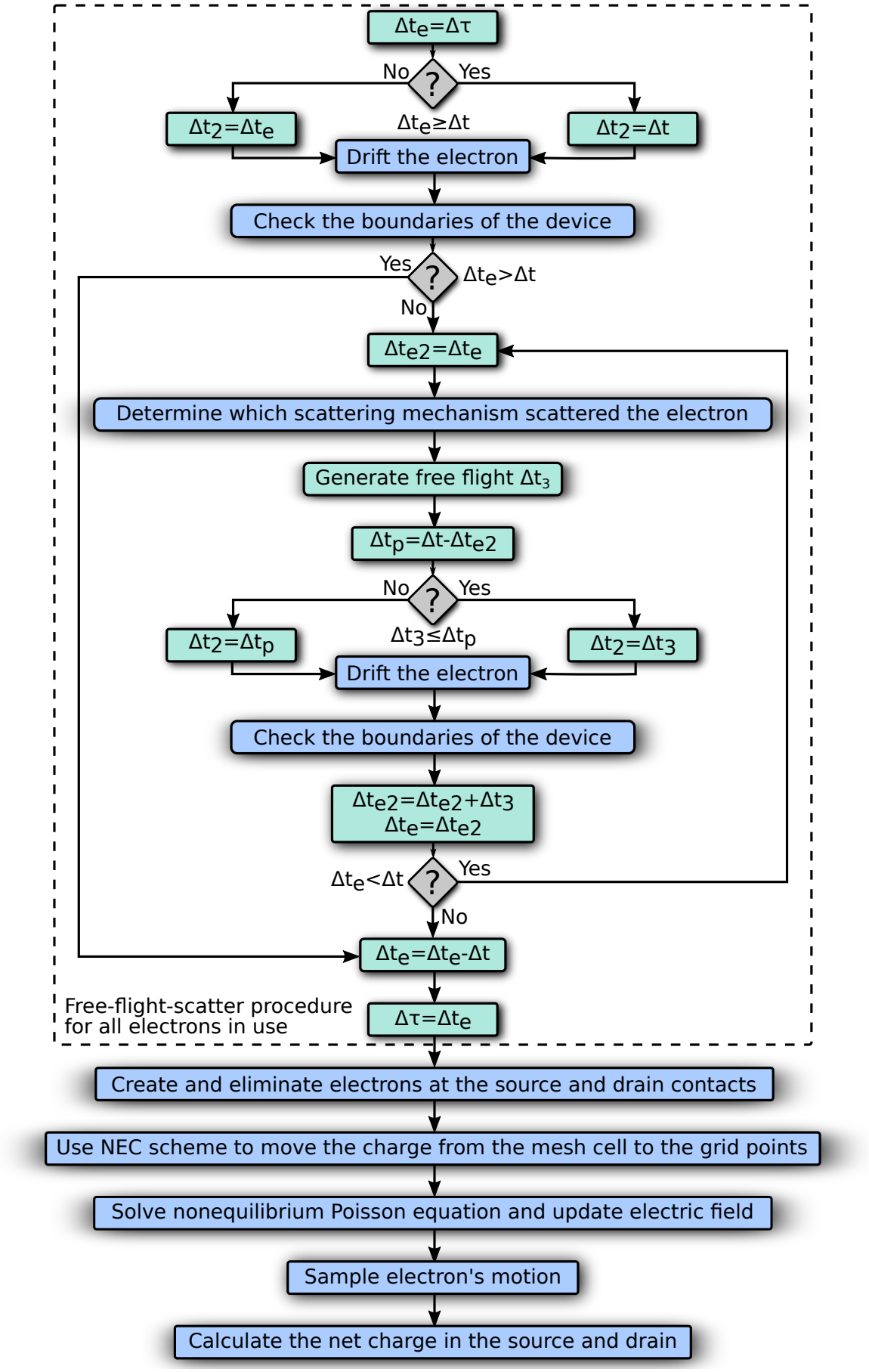

Figure 4: Monte Carlo procedure flowchart for one iteration in a MOSFET device.

2.2 Two-Dimensional Poisson's Equation

The two-dimensional Poisson's equation is:

$$\nabla^2\phi(x,y) = -\frac{q}{\varepsilon}(p(x,y) - n(x,y) + N_D^+ - N_A^-) = -\frac{\rho(x,y)}{\varepsilon}, \tag{3}$$

where $\phi(x,y)$ is the electrostatic potential, q is the elementary charge, ε is the dielectric constant for the material, $n(x,y)$ and $p(x,y)$ are the electron and hole charge densities respectively, N_D^+ and N_A^- are the concentrations of ionized donors and acceptors respectively, and $\rho(x,y)$ is the space charge density [4, 7, 8]. The electron and hole densities are classically calculated as:

$$\begin{aligned} n(x,y) &= n_i e^{\frac{-\phi(x,y)}{k_B T/q}}, \\ p(x,y) &= n_i e^{\frac{-\phi(x,y)}{k_B T/q}}, \end{aligned} \tag{4}$$

where n_i is the intrinsic carrier concentration, k_B is Boltzmann's constant, and T is the temperature [7, 8]. In order to solve the two-dimensional Poisson's equation, it must first be discretized using the finite-difference approximation, which leads to the five-point stencil in two dimensions, as seen in Figure 5 [8–10]. Applying the finite-difference discretization to Poisson's equation in the bulk region of the MOSFET and using the five-point stencil scheme, the five-point difference equation is obtained [10]:

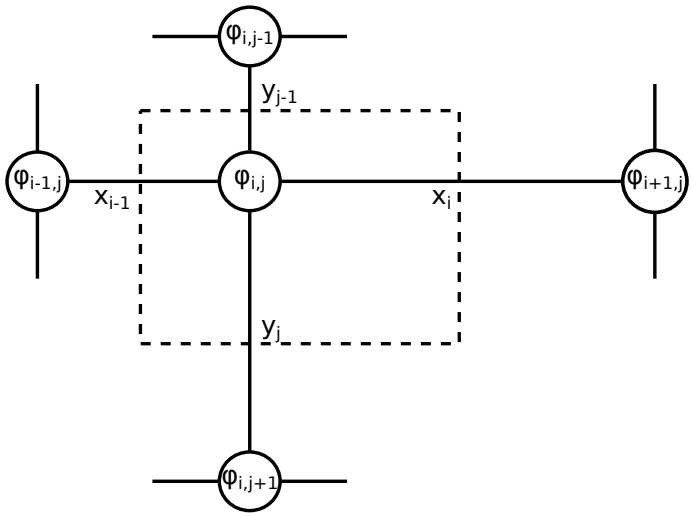

Figure 5: Two-dimensional five-point stencil scheme used for the finite-difference discretization of the two-dimensional Poisson's equation.

$$a_{i,j}\phi_{i+1,j} + b_{i,j}\phi_{i-1,j} + d_{i,j}\phi_{i,j+1} + e_{i,j}\phi_{i,j-1} - c_{i,j}\phi_{i,j} = \alpha\rho_{i,j}, \tag{5}$$

$$a_{i,j} = \frac{y_j + y_{j-1}}{x_i}, \qquad b_{i,j} = \frac{y_j + y_{j-1}}{x_{i-1}},$$

$$d_{i,j} = \frac{x_i + x_{i-1}}{y_j}, \qquad e_{i,j} = \frac{x_i + x_{i-1}}{y_{j-1}},$$

$$c_{i,j} = a_{i,j} + b_{i,j} + d_{i,j} + e_{i,j}, \qquad \alpha_{i,j} = \frac{(x_i + x_{i-1})(y_j + y_{j-1})}{2},$$

Where x_i and y_j are the current mesh grid spacing in the x and y directions respectively, $\frac{x_i+x_{i-1}}{2}$ and $\frac{y_j+y_{j-1}}{2}$ are the change in the mesh grid spacing in the x and y directions (dx, dy) respectively, and $a_{i,j}$, $b_{i,j}$, $d_{i,j}$, $e_{i,j}$, $c_{i,j}$, and $\alpha_{i,j}$ are Poisson's coefficients [8–10]. Additionally, at the boundaries of the device Neumann boundary conditions are used, changing Poisson's coefficients to [11]:

$$\begin{aligned}
x = 0 \quad &: \quad a_{i,j} = 2a_{i,j}, \qquad b_{i,j} = 0, \\
x = x_{max} \, &: \quad a_{i,j} = 0, \qquad b_{i,j} = 2b_{i,j}, \\
y = 0 \quad &: \quad d_{i,j} = 2d_{i,j}, \qquad e_{i,j} = 0, \\
y = y_{max} \, &: \quad d_{i,j} = 0, \qquad e_{i,j} = 2e_{i,j},
\end{aligned} \tag{6}$$

However, at the ohmic contacts of the device Dirichlet boundary conditions are used, changing Poisson's coefficients for equation (5) to [11]:

$$a_{i,j} = b_{i,j} = d_{i,j} = e_{i,j} = 0, \qquad c_{i,j} = 1, \tag{7}$$

Unlike in the bulk Si of the MOSFET, at the Si-SiO_2 interface the dielectric constant is position dependent due to the two different materials at the interface, and therefore the finite-difference discretization of Poisson's equation will differ from equation (5). Using Gauss' law the following relationship between the electric fields in the device is determined [11]:

$$\varepsilon_{ox}E_{ox} - \varepsilon_{si}E_{si} = Q_{int}, \tag{8}$$

where ε_{si} and ε_{ox} are the dielectric constants in Si and SiO_2 respectively, E_{si} and E_{ox} are the transverse electric fields in Si and SiO_2 respectively, and Q_{int} is the charge at the Si-SiO_2 interface [11, 12]. Assuming the Si-SiO_2 interface to be ideal with no charges located at the interface, $Q_{int} = 0$, the equation becomes [12]:

$$\varepsilon_{ox}E_{ox} = \varepsilon_{si}E_{si}, \tag{9}$$

For an ideal insulator, meaning there is no charge located inside the oxide, the transverse electric field is:

$$E_{ox} = \frac{\phi_{ox}}{t_{ox}}, \tag{10}$$

where ϕ_{ox} is the potential drop across the oxide and t_{ox} is the oxide thickness [11, 12]. Additionally, the transverse electric field in the silicon is:

$$E_{si} = \frac{\partial \phi(x,y)}{\partial y} = \frac{\phi_{i,j+1} - \phi_{i,j}}{y_j}, \tag{11}$$

Assuming an ideal MOSFET with no contact potential between the metal and semiconductor, the gate voltage drops partially across the oxide and the semiconductor and becomes:

$$V_G = \phi_{ox} + \phi_s, \tag{12}$$

where V_G is the voltage at the gate, and ϕ_s is the surface potential drop across the silicon [12]. Plugging equations (10)-(12) into equation (9), and rearranging the terms the equation becomes:

$$\frac{\gamma(V_G - \phi_s)}{t_{ox}} = \frac{\phi_{i,j+1} - \phi_{i,j}}{y_j}, \qquad \gamma = \frac{\varepsilon_{ox}}{\varepsilon_{si}}, \tag{13}$$

which leads to the oxide part of the transverse aspect of the potential:

$$\beta_i = \frac{\gamma y_j (V_G - \phi_s)}{t_{ox}}, \tag{14}$$

Plugging the Si and SiO_2 transverse potentials into the transverse part of Poisson's equation, the finite-difference discretization of Poisson's equation at the Si-SiO_2 interface becomes:

$$\begin{aligned}
&a_{i,j}\phi_{i+1,j} + b_{i,j}\phi_{i-1,j} + d_{i,j}(\phi_{i,j+1} + \beta_i) - c_{i,j}\phi_{i,j} = \alpha\rho_{i,j}, \\
&a_{i,j} = \frac{y_j}{x_i}, \qquad\qquad b_{i,j} = \frac{y_j}{x_{i-1}}, \\
&d_{i,j} = \frac{x_i + x_{i-1}}{y_j}, \qquad\qquad e_{i,j} = 0, \\
&c_{i,j} = a_{i,j} + b_{i,j} + d_{i,j}(1 + \frac{\gamma y_j}{t_{ox}}), \qquad \alpha_{i,j} = \frac{(x_i + x_{i-1})(y_j)}{2},
\end{aligned} \tag{15}$$

Since the Si-Sio_2 interface is a line and therefore one-dimensional, the y-direction does not vary and the five-point stencil scheme at the interface no longer includes y_{j-1} nor $\phi_{i,j-1}$, therefore making $dy = y_j$, and changing Poisson's coefficients to those in equation (15).

After the two-dimensional Poisson's equation has been discretized, it is then solved iteratively using the successive over-relaxation (SOR) method to solve for the new po-

tential. The SOR method is a variation of the Gauss-Seidel method for solving Poisson's equation that is used in order to save computation time when running the simulation, since the SOR method improves the rate of convergence when solving Poisson's equation [4, 13]. The general form of the SOR method for a non-uniform mesh for the bulk region of the MOSFET is [10]:

$$\phi_{i,j}^{n+1} = (1-\omega)\phi_{i,j}^{n} + \frac{\omega}{c_{i,j}}[a_{i,j}\phi_{i+1,j}^{n} + b_{i,j}\phi_{i-1,j}^{n+1} + d_{i,j}\phi_{i,j+1}^{n} + e_{i,j}\phi_{i,j-1}^{n+1} + \alpha_{i,j}\rho_{i,j}], \qquad 0 < \omega \leq 2, \tag{16}$$

where $\phi_{i,j}^{n+1}$ is the new potential, $\phi_{i,j}^{n}$ is the old potential, $\frac{1}{c_{i,j}}[a_{i,j}\phi_{i+1,j}^{n} + b_{i,j}\phi_{i-1,j}^{n+1} + d_{i,j}\phi_{i,j+1}^{n} + e_{i,j}\phi_{i,j-1}^{n+1} + \alpha_{i,j}\rho_{i,j}]$ is the standard Gauss-Seidel method, and ω is the weight factor or relaxation factor in order to improve convergence [4, 10, 13]. When $\omega > 1$ the system is over-relaxed and the Gauss-Seidel part is weighted more heavily, and if $\omega < 1$ the system is under-relaxed and $\phi_{i,j}^{n}$ is weighted more heavily; this is done to weight the value closer to the solution in order to improve convergence [4]. However, if ω=1 the equation is not weighted and the standard Gauss-Seidel method is used [4]. Additionally, due to charge neutrality, at the ohmic contacts in the device $\rho_{i,j} = 0$; therefore, the potential does not change at the ohmic contacts [8, 9, 11]. At the Si-SiO2 interface in the MOSFET, the SOR method equation is the same as for a bulk MOSFET, except that the finite-difference discretization equation for the Si-SiO_2 interface is used in the Gauss-Seidel method part of the SOR equation instead of the finite-difference discretization equation for the bulk. The two-dimensional Poisson's equation is calculated once when the device is in equilibrium and then iteratively during the ensemble Monte Carlo method when the device is no longer in equilibrium.

2.3 Initialization

When modeling a MOSFET, the first aspect of the simulation is the initialization steps. All of the necessary constants must be set and the specific material parameter constants must be set to the appropriate values for Si and SiO_2 [4]. Additionally, the dimensions of the specific device being simulated as described in section 1.2 must be set. Also, other constant parameters specifically needed for the simulation must be set such as the time step and the total time of the simulation [4]. Once all of the constants are initialized then the MOSFET device is sectioned off into a rectangular mesh grid with mesh cells of either uniform 1 nm×1 nm or 0.5 nm×0.5 nm mesh sizes for a 250 nm channel MOSFET or a non-uniform mesh with a minimum mesh size of 2 Å and a maximum mesh size of 1 nm. These mesh cells allow the simulation to perform calculations throughout the device one mesh cell at a time. Next the regions of the device are determined and flagged, such as ohmic contacts which are the source, drain, and substrate contacts, the Si-SiO_2 interface, and the bulk. The doping in these different regions as defined

in section 1.2 are also defined in the MOSFET [4]. Next the coefficients for the two-dimensional Poisson's equation are calculated for each region of the device and the initial potential is calculated [4]. Afterward the scattering rates for acoustic, intervalley, and Coulomb scattering processes are calculated from Fermi's Golden rule [4]. Then the two-dimensional Poisson's equation is solved through each region for the equilibrium case where voltage is not applied to the source, drain, or substrate, as described in detail in section 2.2.

After the two-dimensional Poisson's equation in equilibrium reaches convergence, the electric field is updated from the new potential just calculated and the electrons are initialized [4]. During the electron initialization, a starting number of electrons is chosen for the device simulation and the electrons are distributed into the mesh cells throughout the device according to the specified density [4]. The density of the electrons in each mesh cell is calculated using the potential that was calculated by solving the two-dimensional Poisson's equation in equilibrium [4]. Each electron is then given a starting position within the device, an initial random wavevector, a time constant, and a starting energy [4]. Since there is rarely the same correspondence between the number of electrons in the simulation and the number of electrons in an actual MOSFET device, for simplicity each electron as well as other particles throughout the device can be represented as super-particles in the simulation [6]. Each super-particle represents a finite number of actual particles in the device [4]. The charge corresponding to each super-particle is weighted appropriately to the number of particles that it represents [6]. Throughout the course of this paper when mentioning an electron in a discussion of the simulation, it is actually a super-particle instead of a single electron. Once the electrons are initialized, voltage is applied to the terminals of the device so the device is no longer in equilibrium and the ensemble Monte Carlo procedure iteration is conducted, as described in more detail in section 2.1 [4].

3 Modeling Surface-Roughness Scattering

3.1 Constant Specularity Parameter

Simulating the surface-roughness scattering of electrons inside of a MOSFET can be done by using a simple model. Generally when scattering off of a perfectly smooth surface, particles will scatter specularly [5, 18, 19]. When an electron scatters specularly from the Si-SiO_2 interface, the direction of the electron's y component of the wavevector trajectory is flipped when it hits the perfectly smooth surface, as can be seen in Figure 6. However, in order to simulate that the surface at the Si-SiO_2 interface is rough from this method the electron must have the potential to scatter diffusely as well, as shown in Figure 6 [18, 19].

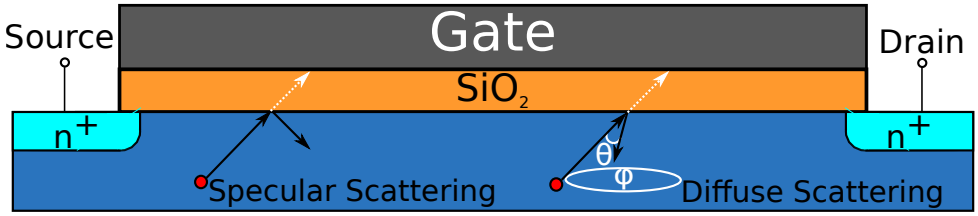

Figure 6: Schematic of the top section of a MOSFET where the Si-SiO_2 interface is perfectly smooth, and the electron can either scatter from the oxide specularly or diffusely.

A constant specularity parameter p, between 0 and 1, can be chosen to determine the probability if the electron scatters specularly [19, 20]. During the simulation, a random number uniformly distributed between 0 and 1 is chosen and compared with the constant specularity parameter; if it is less than or equal to the specularity parameter then the electron scatters specularly. If the electron scatters specularly the magnitude is unchanged and the new direction is determined by:

$$k_y = -k_y, \tag{17}$$

where k_y is the component of the wavevector in the y direction [4]. Since flux is automatically conserved for specular scattering the polar and azimuthal angles do not change [21]. Otherwise if the random number is greater than p the electron scatters diffusely with a probability of $1-p$; however, for diffuse scattering flux is not automatically conserved as it is for specular scattering and the polar and azimuthal angles must change to conserve flux [21]. In order for the flux to be conserved, the flux that enters the surface must be equal to the flux that exits [20–22]. Using the inversion method to generate the random

number used for flux conversion [23]:

$$r(\theta) = \frac{\int_0^{\theta} \cos\theta \sin\theta d\theta}{\int_0^{\frac{\pi}{2}} \cos\theta \sin\theta d\theta} = \sin^2\theta, \tag{18}$$

where the numerator is the entering flux and the denominator is the exiting flux, and $r(\theta)$ is a random number between 0 and 1, and θ is the polar angle [21–23]. Integrating the equation for θ and for ϕ and inverting the solution the electron's new angles are:

$$\theta = \sin^{-1}(\sqrt{r(\theta)}), \tag{19}$$

$$\phi = 2\pi r(\phi), \tag{20}$$

where $r(\theta)$ and $r(\phi)$ are random numbers between 0 and 1. The azimuthal angle has a full 360 degree range, as is expected. However, the polar angle only has a range of 90 degrees in order to conserve the flux, as shown in Figure 6 and Figure 7 [21].Using these values the electron's new direction and magnitude is determined from:

$$\vec{k} = \sqrt{k_x^2 + k_y^2 + k_z^2}, \tag{21}$$

$$k_x = \vec{k}\sin\theta\cos\phi, \tag{22}$$

$$k_y = \vec{k}\cos\theta, \tag{23}$$

$$k_z = \vec{k}\sin\theta\sin\phi, \tag{24}$$

where $\vec{k}$ is the wavevector, k_x is the component of the wavevector in the x direction, k_y is the component of the wavevector in the y direction, k_z is the component of the wavevector in the z direction, and r is a random number between 0 and 1, as is shown in Figure 7 [4, 24]. The k_y component of the wavevector is not dependent on the azimuthal angle since it is the dominant part of the wavevector and the direction and magnitude of the y component is straight down.

If the constant specularity parameter is 1, then the electron scattering from the Si-SiO_2 interface is always specular and the MOSFET device will behave as a MOSFET with a perfectly smooth surface [5, 19, 20, 25]. On the other hand, if the constant specularity parameter is 0 then the electrons always scatter diffusely off of the Si-SiO_2 interface and the MOSFET device will behave as if it has a perfectly rough surface [5, 19, 20, 25]. All other constant specularity parameters between these two points, and the roughness of the Si-SiO_2 can be tweaked by simulating the MOSFET device with a constant specularity parameter closer to 0 for a rougher surface or closer to 1 for a smoother surface [5, 19].

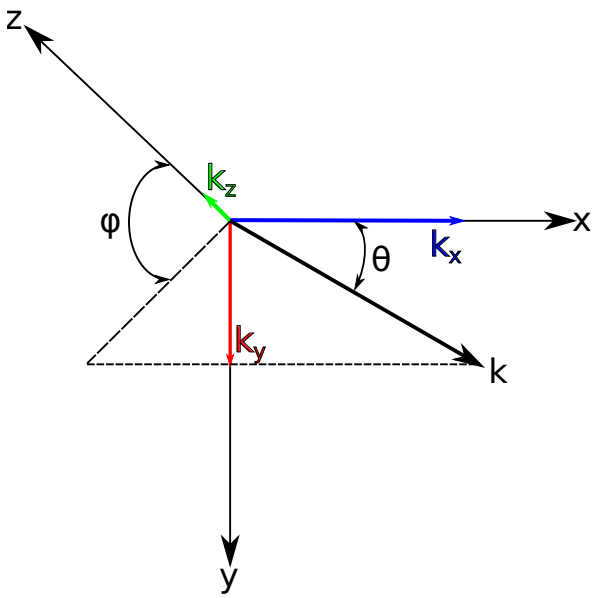

Figure 7: Schematic of the electron coordinate system and wavevector magnitude and direction for a surface-roughness scattering event, where k_x, k_y, and k_z are the wavevector components and θ and ϕ are the polar and azimuthal angles, respectively.

3.2 Momentum-Dependent Specularity Parameter

The height of the rough surface and the momentum of the electron affect the scattering of the electron from the rough interface, so the momentum-dependent specularity parameter is a more robust method for simulating the surface roughness than the constant-specularity-parameter method [5, 20]. The simulation still uses the basic model described in section 3.1 with a perfectly flat surface, as shown in Figure 6. However, instead of a constant specularity parameter, which is manually set and does not vary throughout the Si-SiO_2 surface to determine when the electrons scatter specularly or diffusely, the momentum-dependent specularity parameter is calculated as a function of the momentum of the electron prior to scattering from the Si-SiO_2 interface [20]. The momentum-dependent specularity parameter is derived based on diffraction theory and in the case of no correlation length is:

$$p(k_y) = e^{-(2\Delta k_y)^2}, \tag{25}$$

where k_y is the electron's previous component of the wave vector in the y direction, from equation (23), Δ is the rms roughness height, and $p(k_y)$ is the momentum-dependent specularity parameter [20,25,26]. The roughness of the surface is determined from the rms roughness height, which is generally between 0-5 Å, [27] with 0 rms roughness height being a perfectly smooth surface and 5 Å rms roughness height being a relatively rough surface, and 2 Å being a measured value for rms roughness height for an unintentionally roughened

surface for a MOSFET using HRTEM [1]. Additionally, the specularity parameter is a function of the momentum in the y direction only, since it is the component of the wavevector normal to the rough interface [26]. During the simulation a random number is chosen uniformly between 0 and 1 and compared with the calculated momentum-dependent specularity parameter. If the random number is less than or equal to the momentum-dependent specularity parameter then the electron scatters specularly with a probability of $p(k_y)$. The new direction is chosen as it is done in section 3.1 and the flux is automatically conserved [21]. Otherwise, if the random number is greater than the momentum-dependent specularity parameter then the electron scatters diffusely with a probability of $1 - p(k_y)$ [20, 26].

Similarly to section 3.1 the flux must be conserved, however, since the probability of scattering diffusely is no longer a constant the diffuse scattering distribution is more complex than before. As done in section 3.1 the incoming flux must be equal to the outgoing flux [20–22]:

$$1 - p(k_y) = C(1 - e^{-(2\Delta k_y)^2}) \cos\theta d\theta, \tag{26}$$

where $1 - p(k_y)$ is outgoing distribution from scattering diffusely and the right hand side is the incoming flux, C is a constant, and $d\theta$ is the angle from which the particles are hitting the surface. Then integrating $1 - p(k_y)$ and again using the inversion method [23]:

$$r_\theta = \frac{\int_0^\theta C(1 - e^{-(2\Delta k_y)^2}) \cos\theta \sin\theta d\theta}{\int_0^{\frac{\pi}{2}} C(1 - e^{-(2\Delta k_y)^2}) \cos\theta \sin\theta d\theta}, \tag{27}$$

where the numerator is the incoming flux, the denominator is the outgoing flux, and $r(\theta)$ is a random number between 0 and 1. After integrating and rearranging the terms the formula is then:

$$r_\theta \left(1 - \frac{1 - e^{-(2\Delta\vec{k})^2}}{(2\Delta\vec{k})^2}\right) = \frac{e^{-(2\Delta\vec{k})^2} - e^{-(2\Delta k_y)^2}}{(2\Delta\vec{k})^2} + \sin^2\theta, \tag{28}$$

However, it is not possible to solve for the polar angle θ directly from equation (28), and a numeric method must be used.

The method that was chosen to solve for the polar angle in the MOSFET simulations is Newton's method [28]. However, in order to use Newton's method an initial guess must be chosen for the polar angle which was calculated by expanding the right hand side of equation (28) to the second order in the polar angle [28], which is:

$$(1 - e^{-(2\Delta\vec{k})^2})\theta^2, \tag{29}$$

After setting equation (29) equal to the left hand side of equation (28) and solving for

the polar angle, the initial staring value is calculated to be:

$$\theta \approx \sqrt{r_\theta \left(\frac{1}{1 - e^{-(2\Delta\vec{k})^2}} - \frac{1}{(2\Delta\vec{k})^2} \right)}, \tag{30}$$

which is then plugged into equation (28) for the initial value for Newton's method to numerically solve for the polar angle [28]. Newton's method for numerical analysis is:

$$\theta_{new} = \theta_{old} - \frac{f(\theta_{old})}{f'(\theta_{old})}, \tag{31}$$

where θ_{old} is the current guess for the polar angle, f(θ_{old}) is the solution of equation (28) using the current guess for the polar angle, f'(θ_{old}) is solution of the derivative of equation (28) using the current guess for the polar angle, and θ_{new} is the newly calculated polar angle [28]. The polar angle is presumed to converge when:

$$f(\theta_{old}) \leq tolerance, \tag{32}$$

where the tolerance is a preset number close to zero [28]. If equation (31) is not true then the process is repeated until the polar angle converges, which is the reason that even though a smaller tolerance leads to a more accurate solution it also leads to a longer computation time [28]. Calculating the azimuthal angle using this method produces the same distribution as before in equation (20), and the wavevector of the electron after diffusely scattering from the Si-SiO_2 interface is calculated the same way as was done in section 3.1 from equations (21) - (24), with the new polar angle [4, 21, 24].

3.3 Real-Space Roughness

The most accurate approach to simulate the scattering of particles off of a rough surface is to add a real-space rough surface to the simulation. The real-space rough surface can be generated with both a uniform electric field and a varying electric field. In both cases, the simulation uses a real-space rough surface and charged electrons that have Coulomb interactions with the electric field. In the case of the uniform electric field the electrons do not see a varying field, and therefore act as if a flat surface exists. With the varying electric field, the electrons scatter from the varying electric field created by the real-space rough surface [1, 3, 5]. Real-space rough surface for an electron for a uniform electric field as well as for a varying electric field can be seen in Figures 8 and 9. However, for the uniform electric field the electron does not observe the rough surface and scatter from the uniform field. For either case, the real-space rough surface is created from a chosen autocorrelation formula.

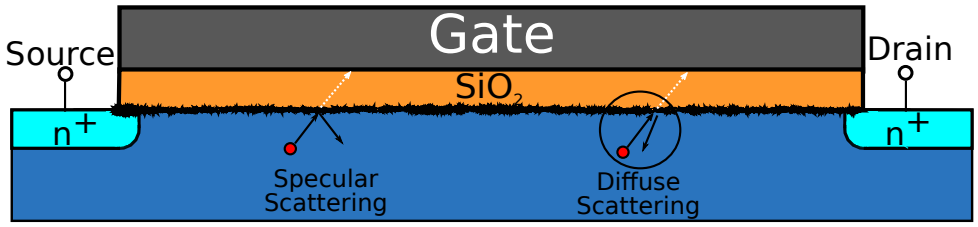

Figure 8: Schematic of a MOSFET with a real-space rough surface at the Si-SiO_2 interface. A magnification of the circled zone in the schematic of the rough surface is demonstrated in Figure 9. The red circle is the electron, the white arrows represent how much the electron would have traveled into the oxide, and the black arrows represent the scattering mechanisms as described in sections 3.1 and 3.2, with a closer look at the diffuse scattering mechanism.

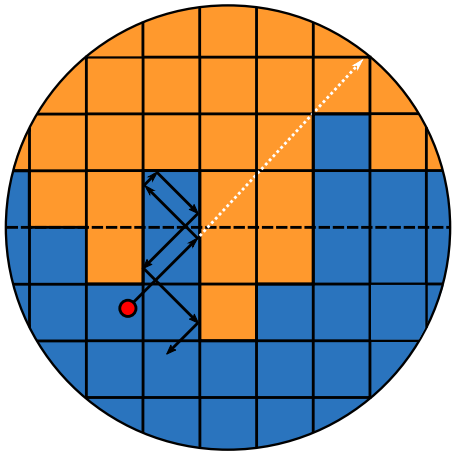

Figure 9: Magnification of the circled region in Figure 8, displaying the movement of an uncharged electron through a random rough region of the Si-SiO_2 interface. The black arrows, which show the electron's path, scatter specularly off of the sides of the rough surface, and the ending position is similar to the aforementioned diffuse scattering mechanism.

Though many different autocorrelation functions could be used, the two most commonly used functions are the Gaussian autocorrelation function:

$$C_{Gaussian}(\vec{r}) = \Delta^2 e^{\frac{-|\vec{r}|^2}{\xi^2}}, \tag{33}$$

and the exponential autocorrelation function:

$$C_{exponential}(\vec{r}) = \Delta^2 e^{\frac{-|\vec{r}|}{\xi}}, \tag{34}$$

where $C(\vec{r})$ is the autocorrelation function, $\vec{r}$ is the position vector, Δ is the rms roughness height, and ξ is the correlation length [1–4, 18, 26, 27]. Goodnick *et al.* measured the roughness using HRTEM, tested the electron transport in several MOSFET devices, and derived the exponential autocorrelation function from their findings. It was determined that the exponential autocorrelation was a more accurate representation of surface roughness in a MOSFET than the previously used Gaussian function [1]. For this reason this

paper will focus on the exponential autocorrelation function. Goodnick *et al.* also measured an rms roughness height of 1.99±0.28 Å and an exponential correlation length of 36.7±23.4 Å on a normally prepared Si(100) sample without adding additional roughness or removing any background order [1]. On the other hand, the authors measured an rms roughness height of 2.82±1.20 Å and an exponential correlation length of 42.1±34.7 Å on intentionally roughened Si(100) without removing any background order, with using hydrochloric acid to roughen the Si-SiO_2 interface further [1].

Generating a rough surface from the exponential autocorrelation function is done by first defining the surface area that needs to have a rough surface, which is defined by $M \times N$, for a rough surface of $Y_{0,k}$, since the roughness height being calculated is in the y direction [27, 29]. The surface area is $x \times z$, the number of rows in the x direction multiplied by the number of columns in the z direction. However, since the MOSFET device is simulated as two-dimensional structures, $M = z = 1$, since there is only the zero column in the z direction, and $N = x = \frac{L}{L_{mesh}}$, where L is the channel length and L_{mesh} is the mesh cell length, which is 0.5 nm for the real-space roughness for the 250-nm device simulation and 2 Å for the 50-nm device simulation, due to the mesh spacing at the interface being the minimum mesh size [27, 29]. The smaller the mesh size the more accurate the rough surface will be compared to an actual rough surface in a MOSFET. The exponential autocorrelation function will be defined as $C_{0,j}(\vec{r})$ by setting $C_{0,N-1-j}(\vec{r})$ for all $j = 0, 1, \cdots, \frac{N}{2} - 1$, and the power spectral density is then found from taking the Fourier transform of the autocorrelation function [27, 29]:

$$\mathscr{F}(C_{0,j}(\vec{r})) = S(q) = \frac{\pi \Delta^2 \xi^2}{\left(1 + \frac{q^2 \xi^2}{2}\right)^{\frac{3}{2}}}, \tag{35}$$

where, $\mathscr{F}(C_{0,j}(\vec{r})$ is the Fourier transform of the autocorrelation function, $S(q)$ is the exponential power spectral density, and q is the scattered wavevector [1–4]. However, since q is not directly known, a fast Fourier transform of the exponential autocorrelation function is used to achieve the power spectral density.

Next, the set of random phases uniformly distributed between 0 and 2π are generated:

$$\begin{aligned} \phi_{0,0} &= \phi_{0,\frac{N}{2}} = 0, \\ \phi_{0,N-j} &= -\phi_{0,j} \qquad j = 0, 1, \cdots, N/2 - 1, \end{aligned} \tag{36}$$

where $\phi_{0,j}$ is the random phase angles matrix, N is the length in the x direction, and j is the current step in the x direction [27, 29]. In order to generate the varying Si-SiO_2 interface height variations and thus create the rough interface, the inverse Fourier

transform of the modified power spectral density must be taken:

$$Y = \mathscr{F}^{-1}(\sqrt{S(q)e^{i\phi}}), \tag{37}$$

where Y is a matrix of the minimum columns in the y direction at the Si-SiO_2 interface, $S(q)$ is the power spectral density, i is the imaginary number, and ϕ is the random phases matrix [27, 29]. The dimensions of the MOSFET device and the y minimum values are then slightly altered in order to verify that the smallest value in the y direction is set to zero instead of a negative number, in order to have positive array indices. The new y minimum values are stored in a matrix and referenced when looping through all of the valid y columns of the MOSFET device in order to prevent the electrons from being initialized inside of a mesh box inside of the oxide.

During the free flight the electron drifts a small amount and its position is compared to the boundaries of the MOSFET device in order to determine if the electron scattered from one of the boundaries of the device [4]. If the electron starting position or ending position of the drift was within range to scatter off of the Si-SiO_2 interface, then the total drift the electron would have taken is divided into smaller sections in order to better determine if the electron reached the Si-SiO_2 surface from any direction. Each electron within range of the interface is checked to determine if it reached the Si-SiO_2 through each section of the drift in order to determine which boundary it scattered off of and which direction it scattered, if it in fact scattered from the Si-SiO_2 interface. With an actual rough surface the electron always scatters specularly, as shown in Figure 6, and therefore flux is always conserved [20]. However, it can scatter specularly off of the x boundary of the Si-SiO_2 interface or off of the y boundary. If it scatters from the x boundary of the Si-SiO_2 interface the electron scatters specularly off of the boundary in the x direction, the new x position is the x boundary it scattered from, the y position is calculated from the ratio of the full drift x and y components, and the x component of the wavevector is flipped for the next drift of the electron:

$$k_x = -k_x, \tag{38}$$

where k_x is the x component of the wavevector [4]. If the electron scatters specularly off of the boundary in the y direction, the new y position is the y boundary it scattered from, the new x position is calculated from the ratio of the full drift x and y components, and the y component of the wavevector is flipped for the next drift, as done in equation (17) [4]. If the electron did not scatter off of the Si-SiO_2 or was not in range of the Si-SiO_2 interface, the side boundaries are checked to determine if the electron scattered off of the sides. Additionally, if the electron did not scatter off the of the Si-SiO_2 interface but hits the top of the source and drain then the electron exited the MOSFET device and it is

removed from the group of active electrons, and it refrains from future drifts [4].

If the electron did scatter off of the Si-SiO_2 interface, the amount left for the electron to drift must be determined. Since the amount of drift for the electron's position is velocity dependent, in order for the new drift to be determined the time the electron took to drift to the boundary that it scattered from must be calculated:

$$dx = h_m(i_v)\langle k_x\rangle\tau \left(1 + af_2 \frac{2hh_m(\left(k_x - \frac{q\tau f_x t_m(i_v)}{\hbar}\right)^2 + \left(k_y - \frac{q\tau f_y t_m(i_v \pm 1)}{\hbar}\right)^2 + k_z^2)}{1 + \sqrt{1 + af_4(\left(k_x - \frac{q\tau f_x t_m(i_v)}{\hbar}\right)^2 + \left(k_y - \frac{q\tau f_y t_m(i_v \pm 1)}{\hbar}\right)^2 + k_z^2)}} \right)^{-1}, \tag{39}$$

where $h_m(i_v)$, $t_m(i_v)$, $t_m(i_v \pm 1)$, and hh_m are relations of the effective masses specific to each of the three valleys, $\langle k_x\rangle$ is the average of the past and present magnitude of the x component of the wavevector, af_2 and af_4 are multiples of the nonparabolicity factor, k_x, k_y, and k_z are the x, y, and z components of the wavevector, q is the charge of an electron, $\hbar$ is Planck's constant, f_x and f_y are the particles electric field in the x and y direction, and τ is the time the electron took in its current drift [4]. Since equation (39) cannot be directly solved for τ, it must be solved numerically as was done in section 3.2 [28]. However, unlike in section 3.2 the derivative of dx is not apparent, so Newton's method is not a valid method to solve for τ and instead the bisection method for numeric analysis is used [28].

The bisection method for numeric analysis is done by first solving for:

$$f(\tau) = h_m(i_v)\langle k_x\rangle\tau \left(1 + af_2 \frac{2hh_m(\left(k_x - \frac{q\tau f_x t_m(i_v)}{\hbar}\right)^2 + \left(k_y - \frac{q\tau f_y t_m(i_v \pm 1)}{\hbar}\right)^2 + k_z^2)}{1 + \sqrt{1 + af_4(\left(k_x - \frac{q\tau f_x t_m(i_v)}{\hbar}\right)^2 + \left(k_y - \frac{q\tau f_y t_m(i_v \pm 1)}{\hbar}\right)^2 + k_z^2)}} \right)^{-1} - dx, \tag{40}$$

where τ is both set to 0 and to the original τ. When τ is set to 0 this τ is referred to as variable a, and when τ is set to the original τ it is referred to as b; these are the two starting values for the bisection method [28]. Additionally, for the bisection method to be a valid method for solving a problem numerically $f(a)$ and $f(b)$ must have opposite signs from one another; for calculating τ, $f(a)$ is negative and $f(b)$ is positive [28]. Once the initial values are calculated and the functions verified, the bisection method algorithm is conducted:

$$c = \frac{a - b}{2}, \tag{41}$$

where a is the minimum potential value for τ and b is the maximum potential value for τ, and c is the bisection of these two points [28]. Afterward $f(c)$ is calculated by plugging c into equation (40). In order to ensure that $f(a)$ and $f(b)$ have opposite signs for the next iteration, if $f(c)$ is negative c is the new value for the variable whose function was

previously negative, in the case of calculating τ, $a = c$, and if $f(c)$ is positive c is the new value for the variable whose function was previously positive, in the case of calculating τ, $b = c$ [28]. The algorithm is then repeated until c converges:

$$f(c) \leq tolerance, \tag{42}$$

where the tolerance is a preset number close to zero [28]. Once the new τ is calculated it is subtracted from the original τ, which is the amount of time the electron has left to drift during its current free flight after having scattered from the Si-SiO_2 interface. The electron drifts again, and the process is repeated for the specified electron until the electron runs out of time for its current drift.

In the case of the uniform electric field, the boundary condition for Poisson's equation is a flat Si-SiO_2 interface at $j = ymin$ throughout the length of the channel. With the electric field kept uniform, the electrons scatter from the field as if from a flat surface. In the case of the varying electric field, the boundary condition for Poisson's equation is a varying Si-SiO_2 interface at $j = ny_{min}(i)$, along the channel. In addition to the interface, the oxide thickness must also vary as a function of $ny_{min}(i)$, due to the real-space roughness, for the electric field to vary properly. Poisson's equation can then be solved as described in section 2.2 for a varying Si-Si_2 interface and oxide thickness, thus allowing for the creation of a varying electric field. With the electric field allowed to vary, the electrons scatter from the varying electric field and observing the rough surface.

4 Simulation Results

4.1 Current and Voltage Calculations

Surface-roughness scattering and other scattering mechanisms degrade the performance of MOSFET devices [30]. The degradation of the current caused by the surface-roughness scattering can be seen in the current–voltage curves [30]. In the simulation, the current was extrapolated by taking the net electrons entering/exiting the source and drain during each time step, multiplying by the normalization factor to obtain the number of actual electrons from the super-particles, multiplying by the charge of a single electron in order to obtain the charge, dividing by the device width to obtain the charge per width, plotting the charges–time steps, and then calculating the slope of the charge–time plot to obtain the source and drain currents per width [4, 31]. However, since the net charge entering/exiting the source and drain per time step is very noisy, a fit line must be used in order to extract the charge throughout the device [31]. In order to fit the charge and therefore calculate the slope, the linear least squares fit (LSF) of the charge-time plot must be taken.

The linear LSF method was implemented by fitting the data points with a straight line:

$$y = mx, \tag{43}$$

where y is the net charges, x is the time steps and m is the slope of the line, which is the value of the current [4,33]. In order to avoid unnecessary variations from the charge–time plot, the line equation was used without a y-intercept. In order to extract the desired line, the sum of the residuals squared must be taken:

$$S = \sum_{i=1}^{n} (y - mx)^2, \tag{44}$$

where n is the number of data points and S is a system of n simulations [32, 33]. The slope is then calculated by differentiating S with respect to the slope:

$$\frac{\partial S}{\partial m} = -2 \sum_{i=1}^{n} x(y - mx) = 0, \tag{45}$$

separating out the terms and solving for the slope the equation is [32, 33]:

$$m = \frac{\sum_{i=1}^{n} xy}{\sum_{i=1}^{n} x^2}, \tag{46}$$

where m is the slope [32] of the charge–time plot, as well as the current through the device from the preset voltages. The current at the drain is extracted in this method in

order to obtain the drain current–drain voltage (I_D-V_D) and drain current–gate voltage (I_D-V_G) graphs. For the I_D-V_D plot, the gate voltage is set to 1V and the drain voltage is swept from 0-1V and for the I_D-V_G the drain voltage is set to 0.4 V and the gate voltage is swept from -0.4-1.2 V.

4.2 Current–Voltage Curves

The MOSFET devices that were simulated for all the various methods are the devices described in section 1.2 using the simulation method described in section 2 and containing acoustic, intervalley, and Coulomb scattering mechanisms in addition to surface-roughness scattering. In order to best compare the current–voltage curves, all methods of surface-roughness scattering were implemented on both devices. For each set of current–voltage curves for both devices the constant specularity parameter of $p = 1$ (perfectly smooth surface) and $p = 0$ (perfectly rough surface) [5, 20] curves for the device are displayed for reference, in order to determine where each specified curve is located in comparison to the two extremes. Since the constant-specularity-parameter method is not the most accurate method for simulating the surface roughness, it is possible to have current–voltage curves below the perfectly rough curve.

4.2.1 250-nm MOSFET Devices

For the 250-nm MOSFET the current–voltage curves obtained from the constant-specularity-parameter method as described in section 3.1 are shown in Figure 10(a) and Figure 10(b). These curves were simulated with $p = 0.5$ (fairly rough surface), as well as the two extreme values, to demonstrate the range of values that can be achieved using the constant-specularity-parameter method. As seen from the large range between the two extremes, the drain current can be drastically decreased due to the amount of scattering from the roughness that is introduced at the Si-SiO_2 interface. Thus, the constant-specularity-parameter method is a valid way to compute the surface-roughness scattering of electrons, since it can display the effects for an actual MOSFET device by modifying the specularity parameter until it matches the experimental data. However, since the constant specularity parameter is a fitting parameter, and not able to reach roughness below $p = 0$, it is not the most robust way to simulate the surface-roughness scattering in a MOSFET.

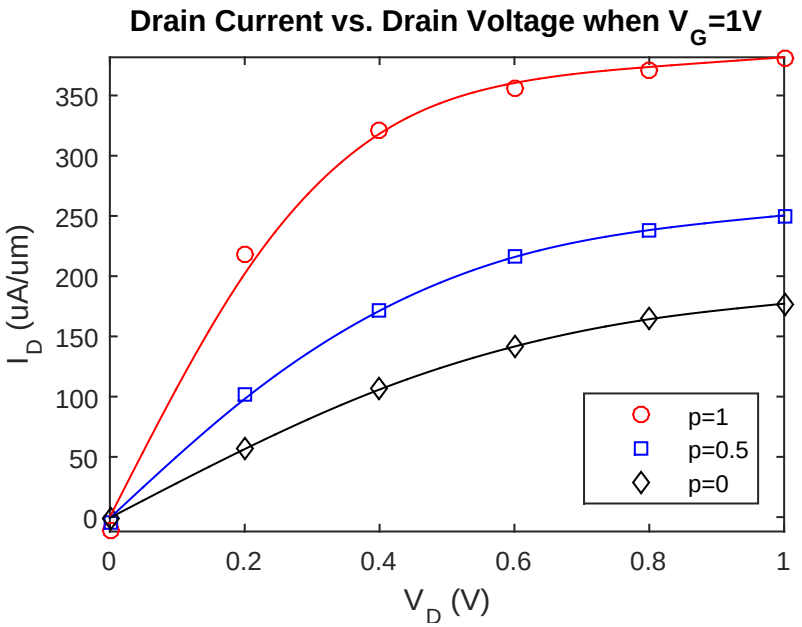

(a)

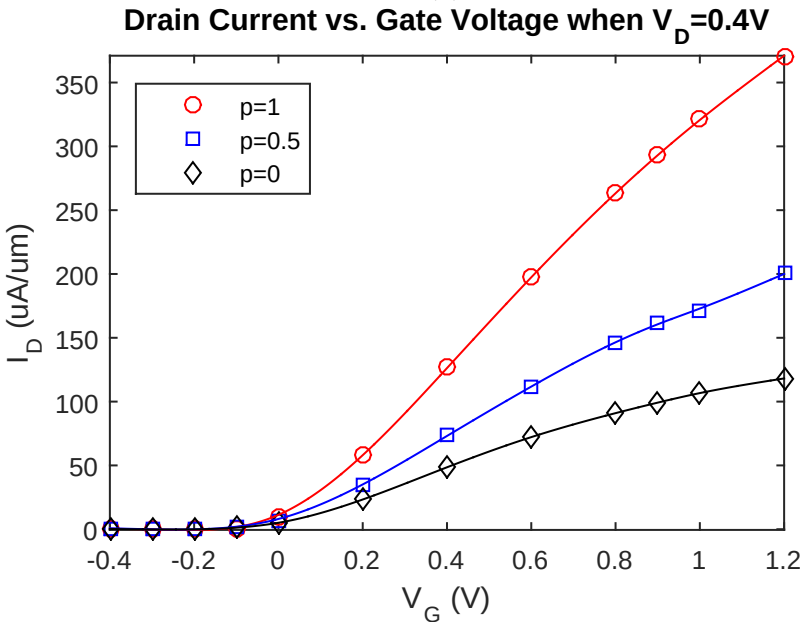

(b)

Figure 10: (a) I_D-V_D and (b) I_D-V_G curves for a 250-nm MOSFET using the constant-specularity-parameter method. The red curves are the current-voltage curves for a perfectly smooth MOSFET, the black curves are for a perfectly rough MOSFET, and the blue curves are a fairly rough MOSFET.

A more robust method used to simulate surface-roughness scattering of electrons in a MOSFET is the momentum-dependent specularity-parameter method, as described in section 3.2, since it uses the actual MOSFET's rms roughness height in order to calculate the specularity parameter. The current–voltage curves for the momentum-dependent specularity-parameter method using an rms roughness height of 2 Å [1] are shown in Figures 11(a) and 11(b).

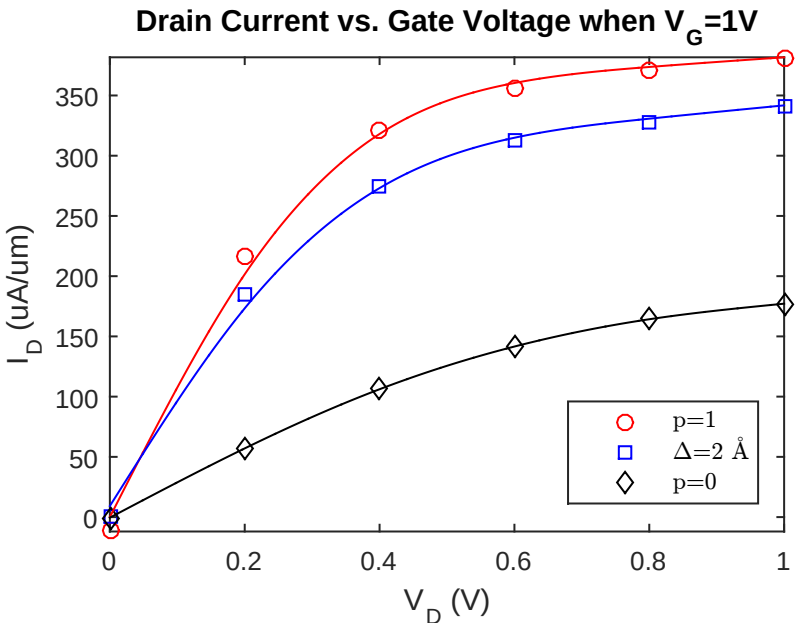

(a)

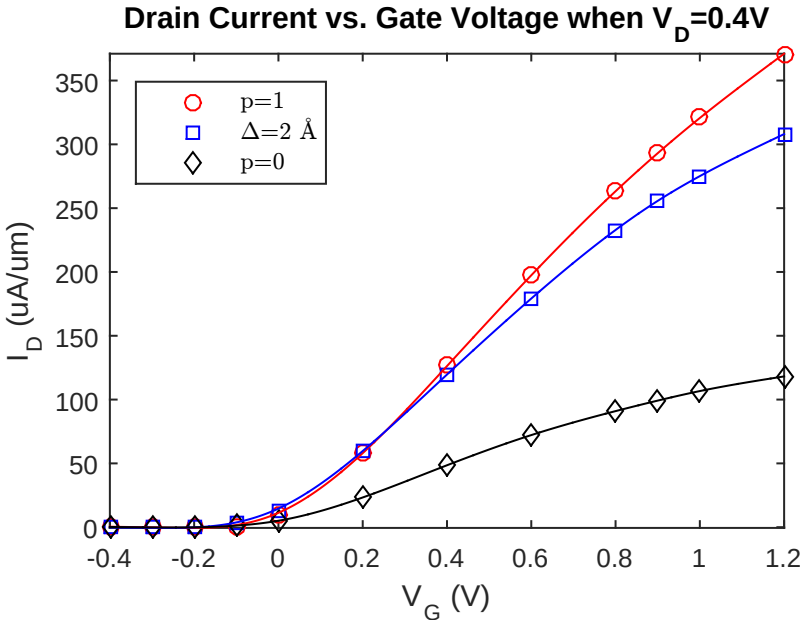

(b)

Figure 11: (a) I_D-V_D and (b) I_D-V_G curves for a 250-nm MOSFET using the momentum-dependent specularity-parameter method with an rms roughness height for an unintentionally roughened MOSFET. The red and black curves display the two extremes, perfectly smooth and rough, respectively, and the blue curves display a MOSFET with a momentum-dependent specularity parameter with rms roughness height of 2 Å.

The current–voltage curves for the momentum-dependent specularity-parameter method using an rms roughness height of 5 Å [1, 27] are shown in Figures 12(a) and 12(b). Both sets of the momentum-dependent specularity-parameter curves are within the two extremes, displaying that the momentum-dependent specularity-parameter methods validity for simulating the surface-roughness scattering of electrons in of a MOSFET. However, it is not the best method for simulating the surface-roughness scattering because the ac-

tual roughness in the MOSFET also depends on the correlation length of the MOSFET.

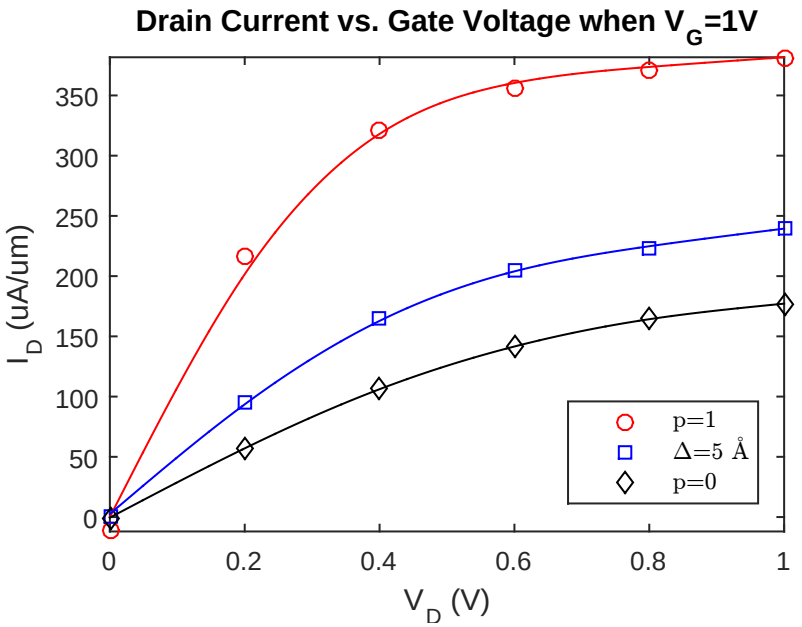

(a)

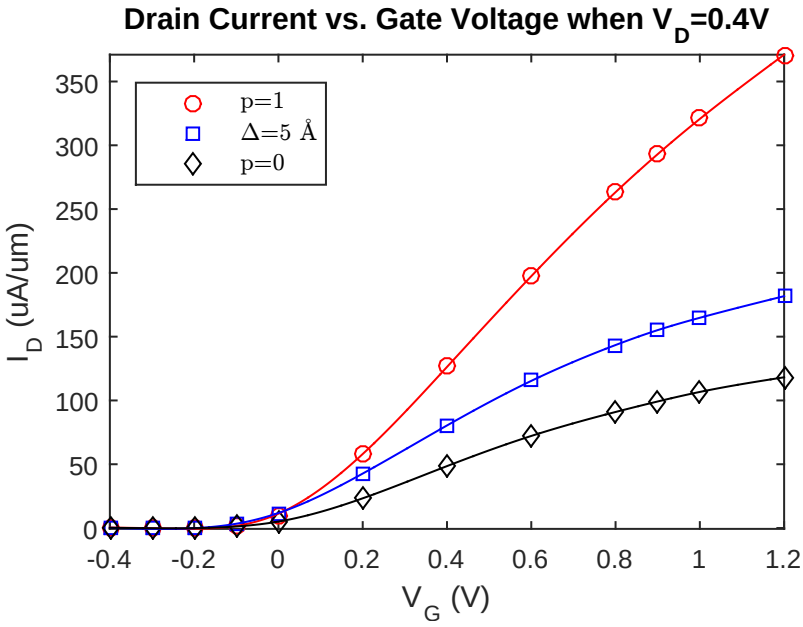

(b)

Figure 12: (a) I_D-V_D and (b) I_D-V_G curves for a 250-nm MOSFET using the momentum-dependent specularity-parameter method with an rms roughness height for an intentionally roughened MOSFET. The red and black curves display the two extremes, perfectly smooth and rough, respectively, and the blue curves display a MOSFET with a momentum-dependent specularity parameter with rms roughness height of 5 Å.

Another method used to simulate surface-roughness scattering in a MOSFET is adding a real-space rough surface with a uniform electric field, as described in section 3.3, since it uses an actual MOSFET's rms roughness height and correlation length in order to generate a real-space rough surface. The current–voltage curves for a MOSFET with

$\Delta = 2$ Å, $\xi = 35$ Å are shown in Figures 13(a) and 13(b). Due to the uniform electric field, the curves are similar to the perfectly smooth curves for the constant-specularity-parameter method, since the electrons scatter from the uniform electric field and not rough surface.

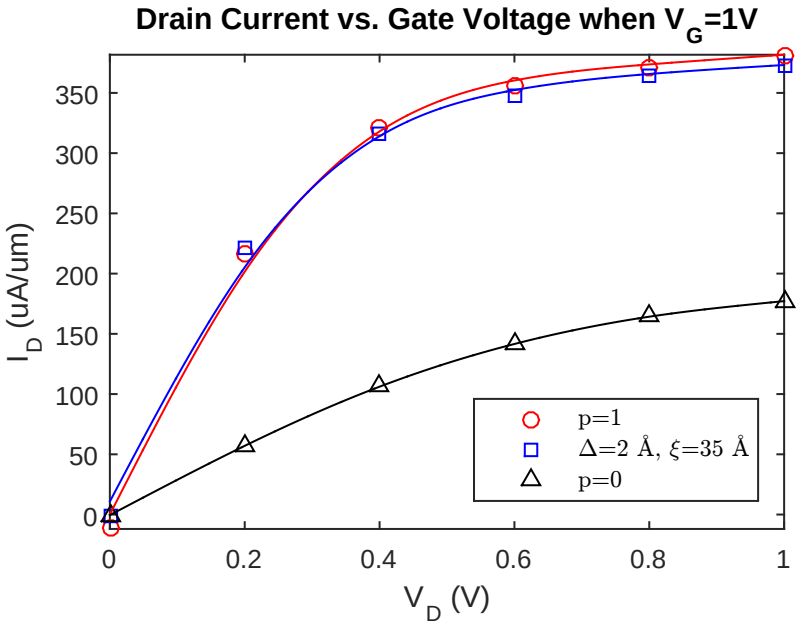

(a)

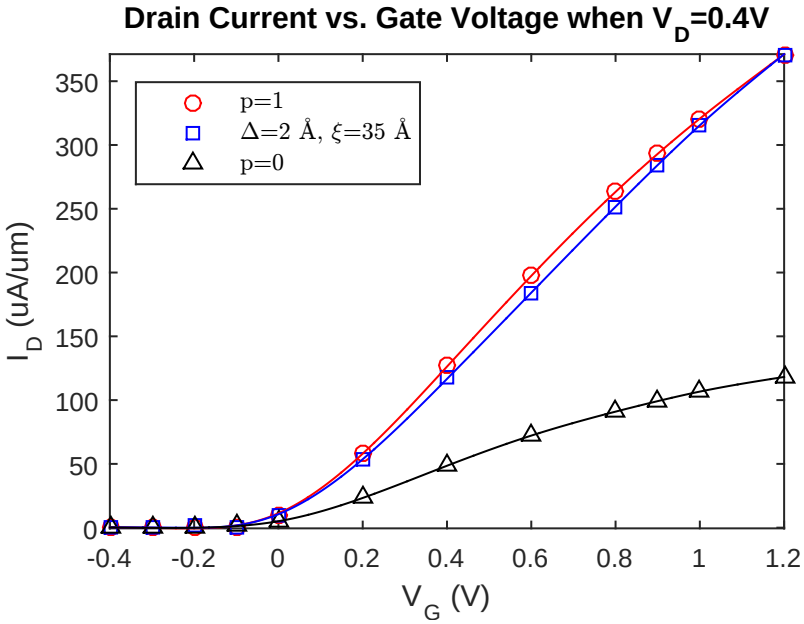

(b)

Figure 13: (a) I_D-V_D and (b) I_D-V_G curves for a MOSFET using the real-space rough-surface method with a uniform electric field, a 0.5 nm mesh, $\Delta = 2$ Å, and $\xi = 35$ Å for a 250-nm MOSFET. The red and black curves display the two extremes, perfectly smooth and rough, respectively, and the blue curves display a MOSFET with roughness generated from an rms roughness height of 2 Å and correlation length of 35 Å.

The most accurate method used to simulate surface-roughness scattering of electrons

in a MOSFET is adding a real-space rough surface with a varying electric field, as described in section 3.3, since it uses an actual MOSFET's rms roughness height and correlation length in order to generate a real-space rough surface, which varies the electric field. The current–voltage curves for an unintentionally roughened MOSFET ($\Delta = 2$ Å, $\xi = 35$ Å) [1] are shown in Figures 14(a) and 14(b).

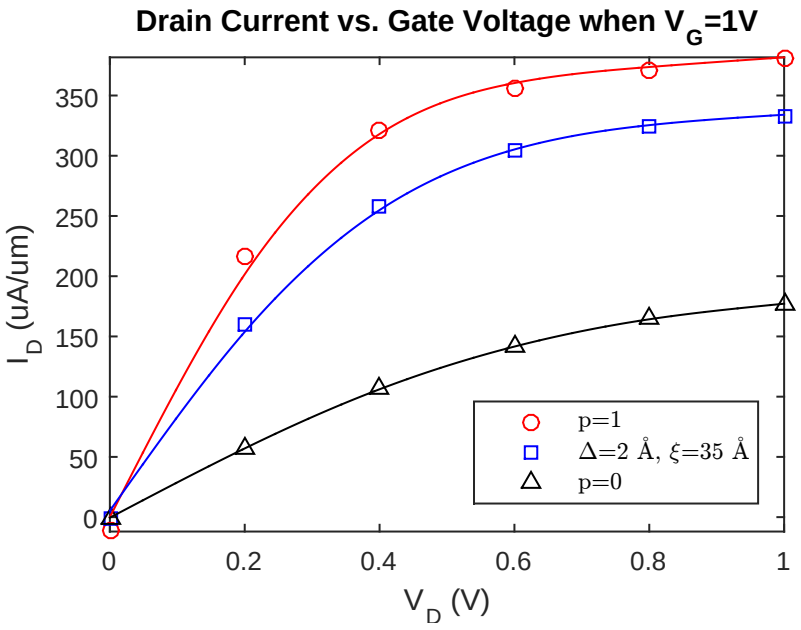

(a)

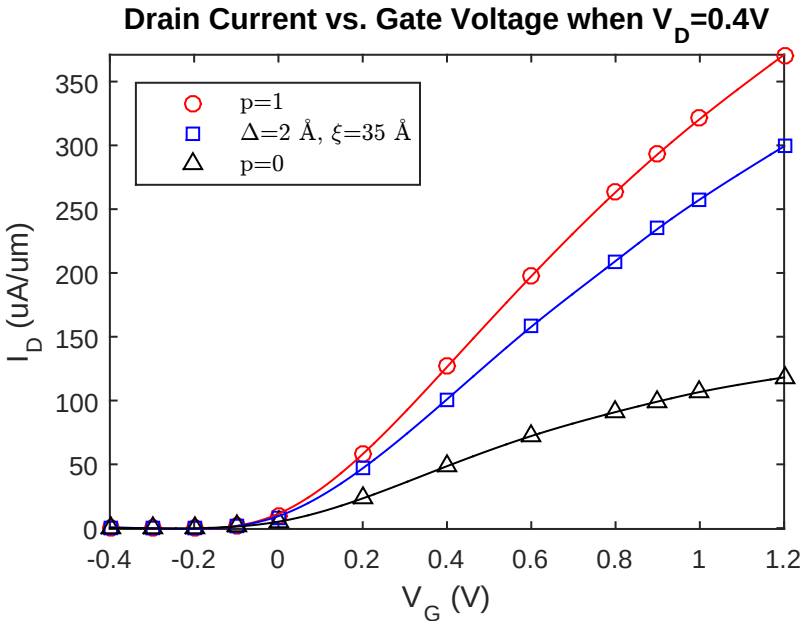

(b)

Figure 14: (a) I_D-V_D and (b) I_D-V_G curves for a 250-nm MOSFET using the real-space rough-surface method with a varying electric field, a 0.5 nm mesh, and an rms roughness height and correlation length for an unintentionally roughened MOSFET. The red and black curves display the two extremes, perfectly smooth and rough, respectively, and the blue curves display a MOSFET with roughness generated from an rms roughness height of 2 Å and correlation length of 35 Å.

The current–voltage curves for an intentionally roughened MOSFET ($\Delta = 3$ Å, $\xi = 40$ Å) [1] are shown in Figures 15(a) and 15(b). Both sets of curves for the real-space roughness with a varying field are within the two extremes, displaying that a real rough surface is a valid method for simulating the surface-roughness scattering of electrons in of a MOSFET.

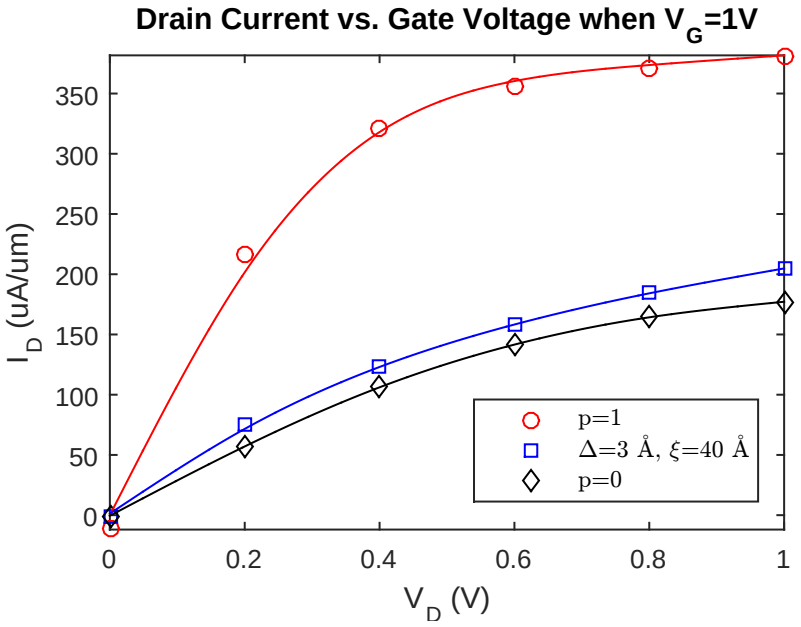

(a)

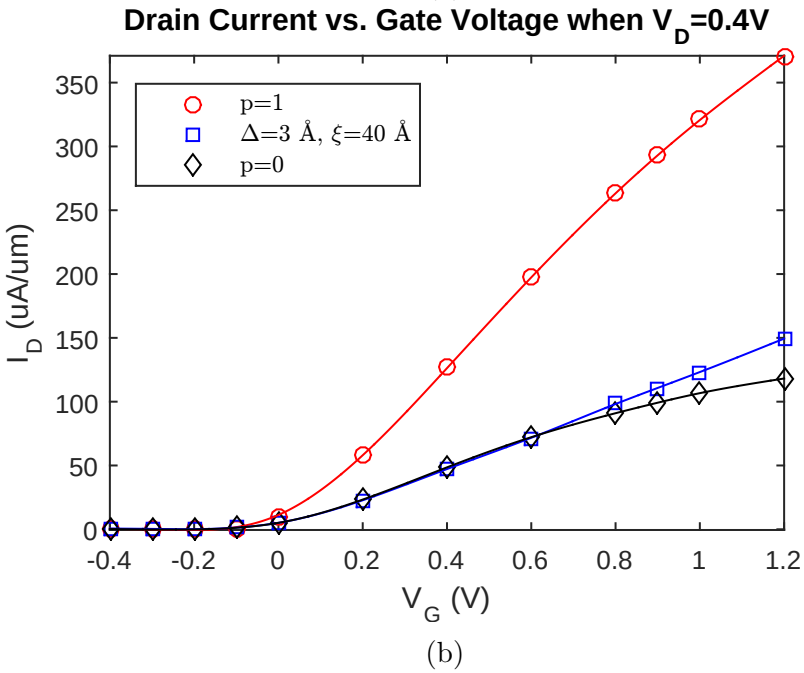

(b)

Figure 15: (a) I_D-V_D and (b) I_D-V_G curves for a 250-nm MOSFET using the real-space rough-surface method with a varying electric field, a 0.5 nm mesh, and an rms roughness height and correlation length for an intentionally roughened MOSFET. The red and black curves display the two extremes, perfectly smooth and rough, respectively, and the blue curves display a MOSFET with roughness generated from an rms roughness height of 3 Å and correlation length of 40 Å.

4.2.2 50-nm MOSFET Devices

The decrease from the 250-nm device to the 50-nm device, while keeping the voltage the same, allows the current through the device to increase; therefore the current vs voltage curves for the 50-nm device are higher than that of the 250-nm device. Additionally, since the 50-nm device is simulated with a non-uniform mesh as opposed to the uniform mesh for the 250-nm device, the surface-roughness scattering of electrons for the 50 -nm device is more accurate than for the 250-nm device since the mesh size near the channel of the device can be made much smaller than for the 250-nm device. The smallest reasonable mesh size achieved for the 250-nm device was 0.5 nm uniform mesh, due to the time limitations required by solving Poisson's equation. On the other hand, the 50-nm device, due to the non-uniform mesh, was able to achieve a 0.2 nm mesh size at the channel of the device with the time limitations. Due to the mesh size limitation for the real-space rough-surface method the surface was only roughened at the ends of the channel and not as much in the middle of the channel. However, due to the decrease in mesh size at the channel the 50-nm device was able to have roughness throughout most of the channel region, making it a more accurate surface-roughness simulation than the 250-nm uniform mesh device simulation. In addition to the non-uniform mesh the 50-nm device has an increased width size from the 250-nm device, which allows more electrons to flow through the device.

For the 50-nm MOSFET the current–voltage curves obtained from the constant specularity-parameter method as described in section 3.1 are shown in Figure 16(a) and Figure 16(b). As was done with the 250-nm device, the constant-specularity-parameter curves were simulated with $p = 0.5$ (fairly rough surface) as well as the two extreme values to demonstrate the range of values that can be achieved using the constant-specularity-parameter method. As before, due to the large range between the extremes the current can be drastically decreased due to surface-roughness scattering, showing the validity of the constant-specularity-parameter method. However, since the constant specularity parameter is a fitting parameter used to vary the roughness until the correct roughness is achieved, it is not the most robust method for simulating surface-roughness scattering in a MOSFET device. Additionally, the constant-specularity-parameter method cannot always simulate the roughness of an actual MOSFET, which can be more rough the perfectly roughened MOSFET simulation using the constant-specularity-parameter method.

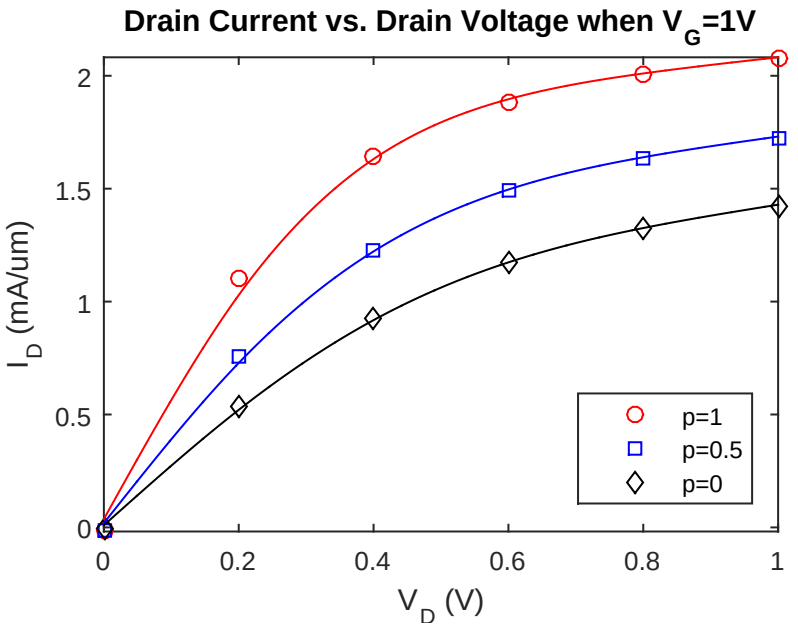

(a)

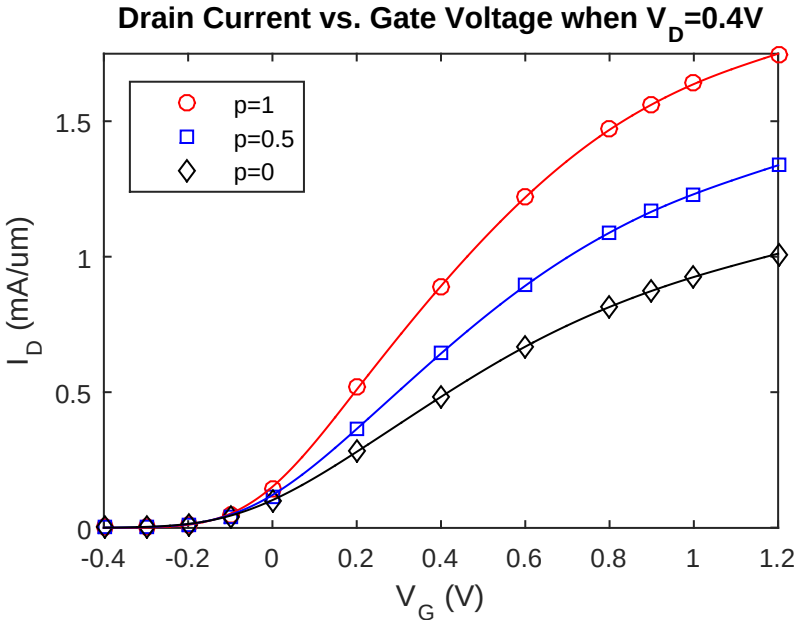

(b)

Figure 16: (a) I_D-V_D and (b) I_D-V_G curves for a 50-nm MOSFET using the constant-specularity-parameter method. The red curves are the current–voltage curves for a perfectly smooth MOSFET, the black curves are for a perfectly rough MOSFET, and the blue curves are a fairly rough MOSFET.

A more robust method used to simulate surface-roughness scattering of electrons in a MOSFET is the momentum-dependent specularity-parameter method, as described in section 3.2, since it uses the actual MOSFET's rms roughness height in order to calculate the specularity parameter. The current–voltage curves for the momentum-dependent specularity-parameter method using an rms roughness height of 2 Å [1] are shown in Figures 17(a) and 17(b).

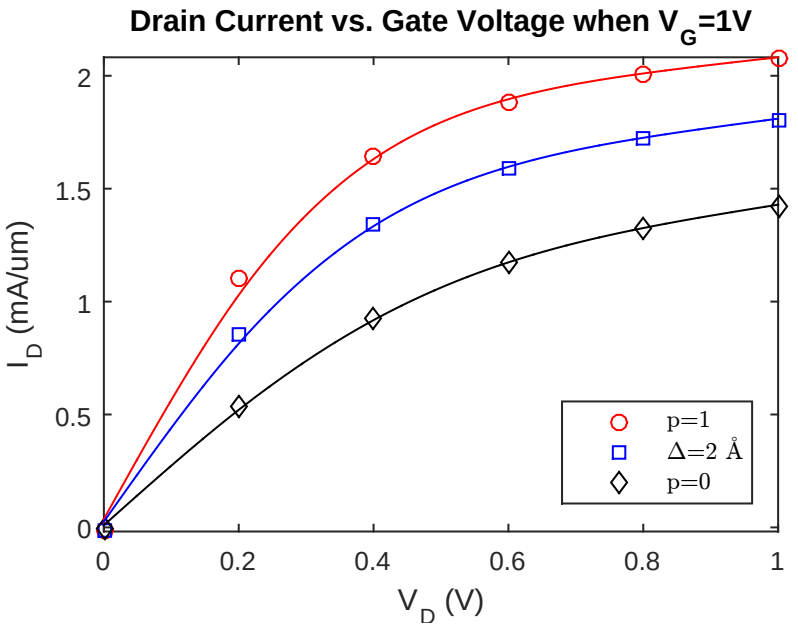

(a)

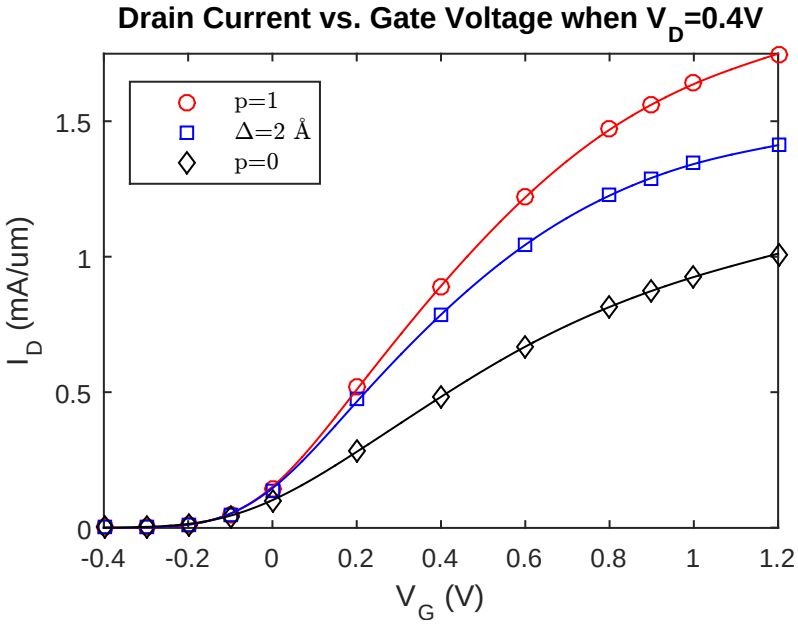

(b)

Figure 17: (a) I_D-V_D and (b) I_D-V_G curves for a 50-nm MOSFET using the momentum-dependent specularity-parameter method with an rms roughness height for an unintentionally roughened MOSFET. The red and black curves display the two extremes, perfectly smooth and rough, respectively, and the blue curves display a MOSFET with a momentum-dependent specularity parameter with rms roughness height of 2 Å

The current–voltage curves for the momentum-dependent specularity-parameter method using an rms roughness height of 5 Å [1,27] are shown in Figures 18(a) and 18(b). As for the 250-nm device, both sets of the momentum-dependent specularity-parameter curves are within the two extremes, displaying that the momentum-dependent specularity-parameter method is a valid method for simulating the surface-roughness scattering of electrons in of a MOSFET. However, it is still not the best method for simulating the

surface-roughness scattering because the actual roughness in the MOSFET is dependent on more than the rms roughness height.

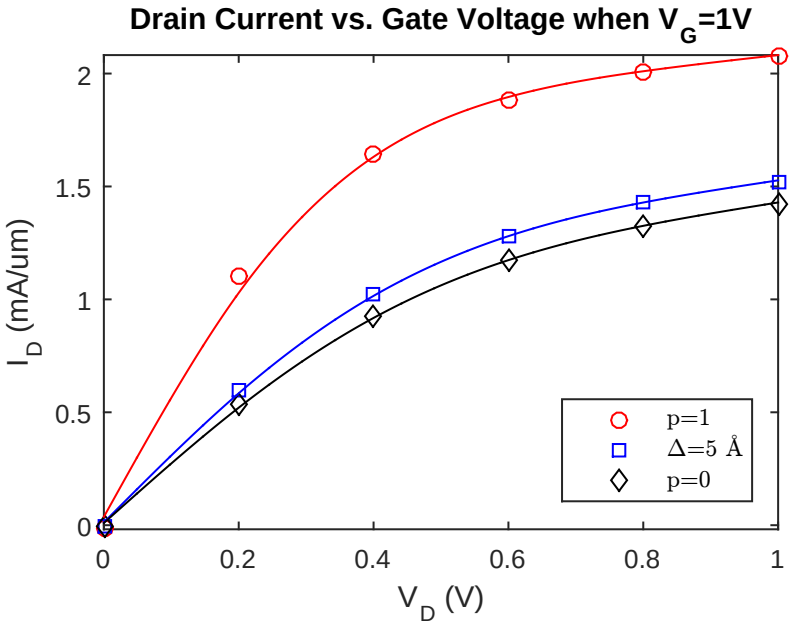

(a)

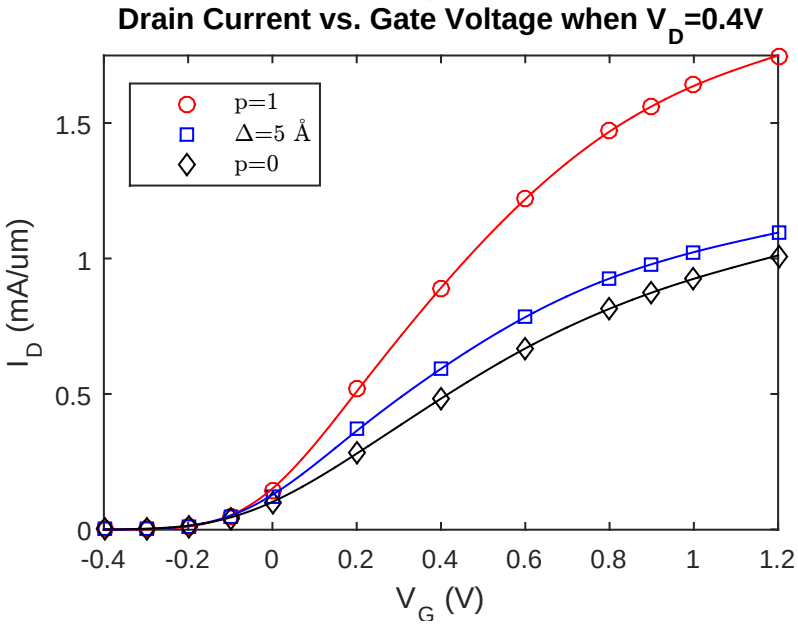

(b)

Figure 18: (a) I_D-V_D and (b) I_D-V_G curves for a 50-nm MOSFET using the momentum-dependent specularity-parameter method with an rms roughness height for an intentionally roughened MOSFET. The red and black curves display the two extremes, perfectly smooth and rough, respectively, and the blue curves display a MOSFET with a momentum-dependent specularity parameter with rms roughness height of 5 Å

Another method used to simulate surface-roughness scattering in a MOSFET is adding a real-space rough surface with a uniform electric field, as described in section 3.3, since it uses an actual MOSFET's rms roughness height and correlation length in order to

generate a real-space rough surface. The current–voltage curves for a MOSFET with $\Delta = 2$ Å, $\xi = 35$ Å are shown in Figures 19(a) and 19(b). As for the 250-nm device, the curves for the real-space rough surface with a uniform electric field are similar to the perfectly smooth curves using the constant-specularity-parameter method.

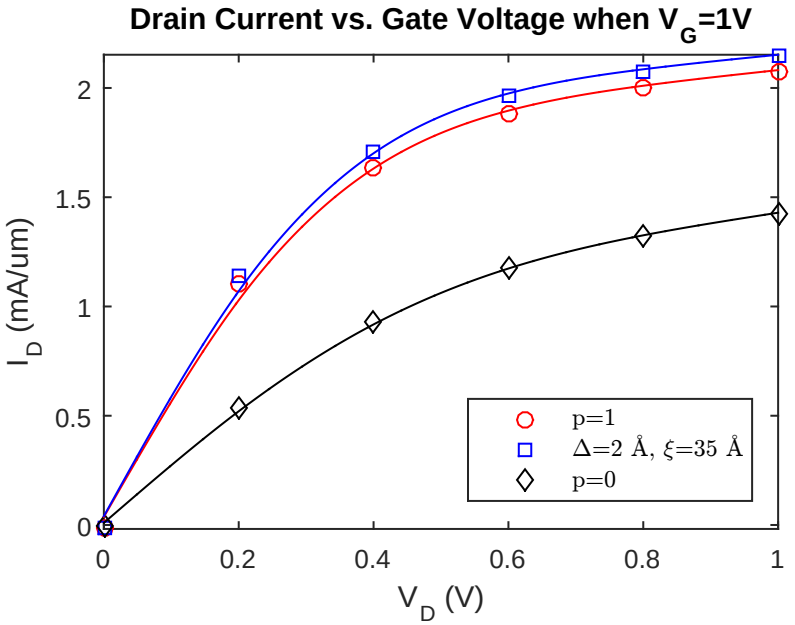

(a)

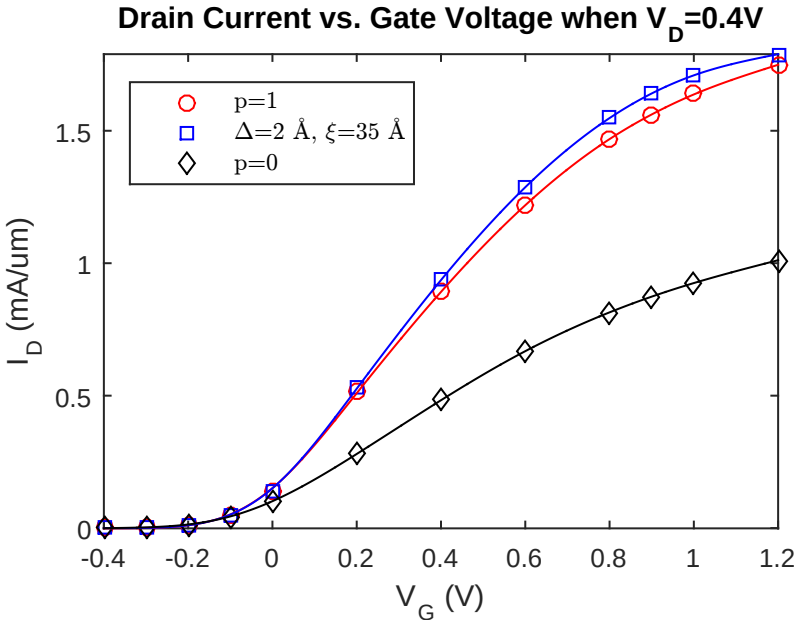

(b)

Figure 19: (a) I_D-V_D and (b) I_D-V_G curves for a MOSFET using the real-space rough-surface method with a uniform electric field, $\Delta = 2$ Å, and $\xi = 35$ Å for a 50-nm MOSFET. The red and black curves display the two extremes, perfectly smooth and rough, respectively, and the blue curves display a MOSFET with roughness generated from an rms roughness height of 2 Å and correlation length of 35 Å.

The most accurate method used to simulate surface-roughness scattering of electrons

in a MOSFET is adding a real-space rough surface with a varying electric field, as described in section 3.3, since it uses an actual MOSFET's rms roughness height and correlation length in order to generate a real-space rough surface, and the electric field varies due to the rough surface. The current–voltage curves for an unintentionally roughened MOSFET ($\Delta = 2$ Å, $\xi = 35$ Å) [1] are shown in Figures 20(a) and 20(b).

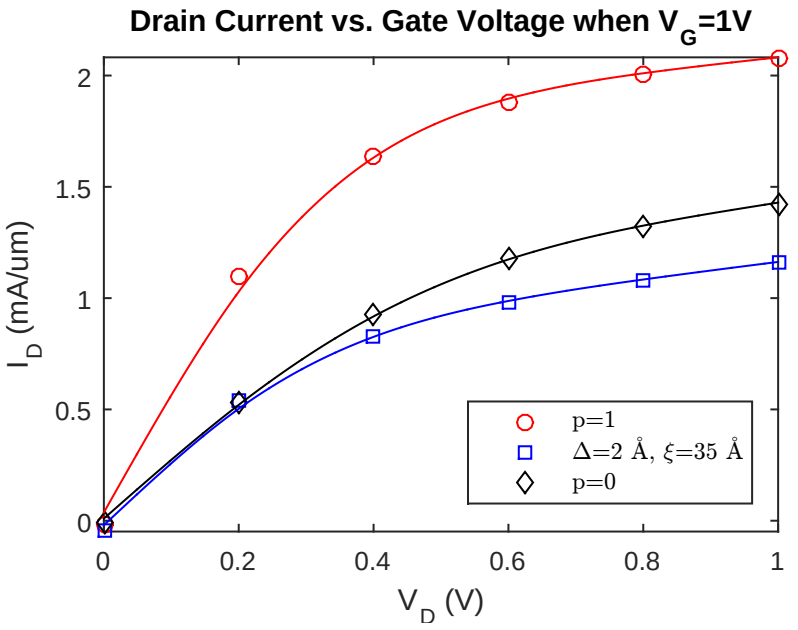

(a)

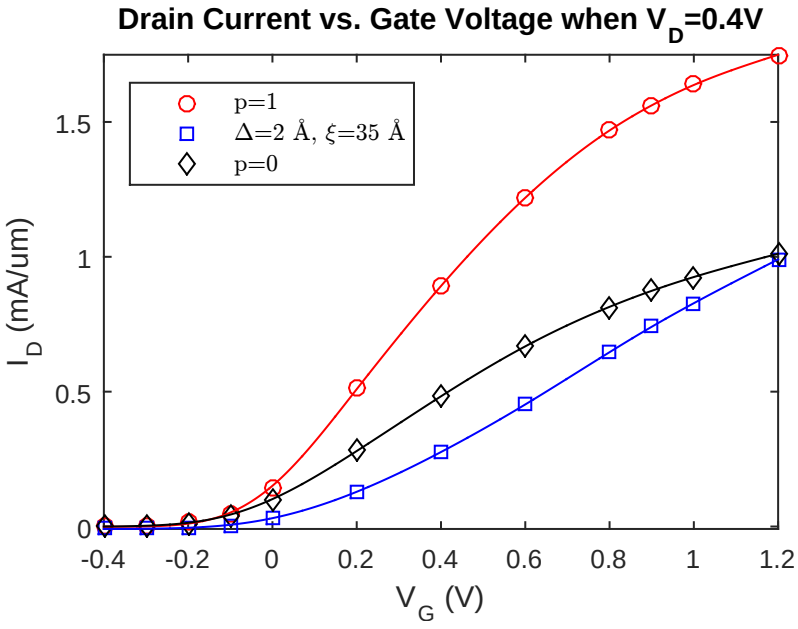

(b)

Figure 20: (a) I_D-V_D and (b) I_D-V_G curves for a 50-nm MOSFET using the real-space rough-surface method with a varying electric field, and an rms roughness height and correlation length for an unintentionally roughened MOSFET. The red and black curves display the two extremes, perfectly smooth and rough, respectively, and the blue curves display a MOSFET with roughness generated from an rms roughness height of 2 Å and correlation length of 35 Å.

The current–voltage curves for an intentionally roughened MOSFET (Δ = 3 Å, ξ = 40 Å) [1] are shown in Figures 21(a) and 21(b). Due to the increased roughness along the channel of the 50-nm device, both sets of curves for the real-space rough surface with a varying electric field method are below the perfectly rough curves, displaying the limitations of the constant-specularity-parameter method.

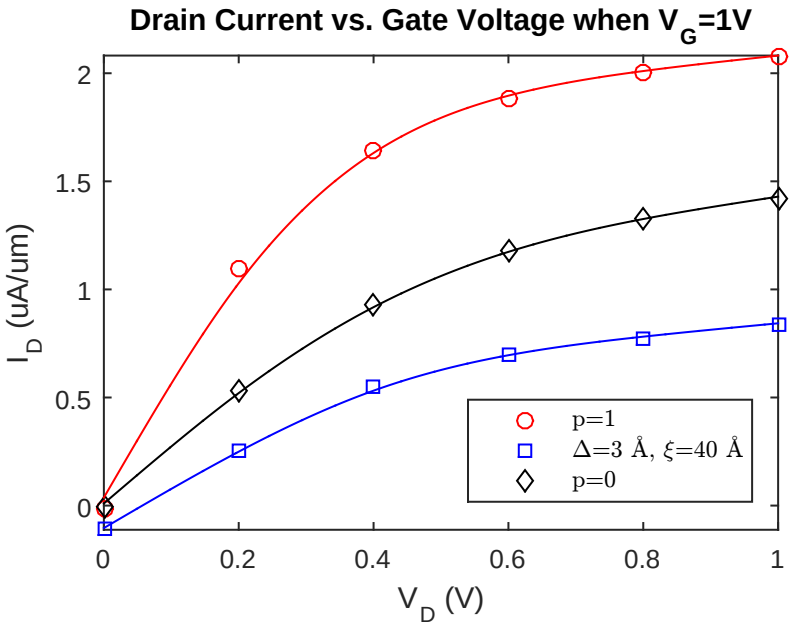

(a)

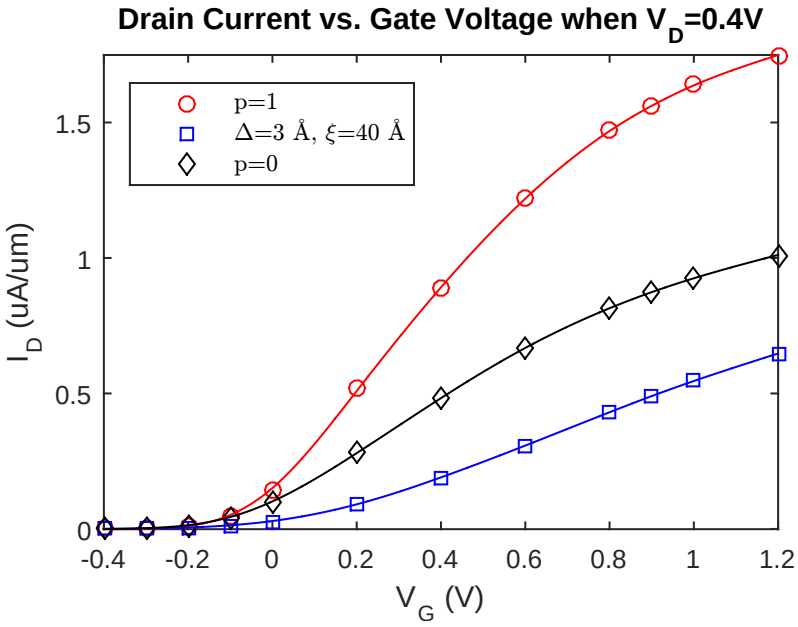

(b)

Figure 21: (a) I_D-V_D and (b) I_D-V_G curves for a 50-nm MOSFET using the real-space rough-surface method with a varying electric field, and an rms roughness height and correlation length for an intentionally roughened MOSFET. The red and black curves display the two extremes, perfectly smooth and rough, respectively, and the blue curves display a MOSFET with roughness generated from an rms roughness height of 3 Å and correlation length of 40 Å.

4.3 Mobility and Electric Field Calculations

Surface-roughness scattering and other scattering mechanisms greatly degrade the current and the electron mobility in MOSFETs [34, 35]. The channel mobility is a measure of how quickly an electron can move from the source to the drain of the device, and scattering slows the electrons down and causes them to take longer to travel from the source to the drain. The degradation of the low-field mobility due to surface-roughness scattering and as other scattering mechanisms can be seen from the mobility–effective electric field curves [34, 35]. A schematic representation of all of the scattering mechanisms and their contribution to the mobility degradation can be seen in Figure 22 [34]. As shown, surface-roughness scattering can greatly degrade the mobility of the device. In the simulation, the channel mobility and effective electric field were extracted using two different methods and compared [38, 40].

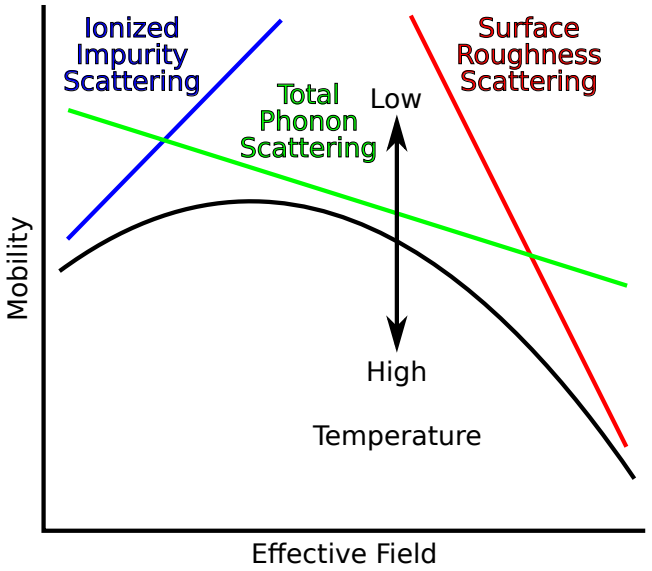

Figure 22: Schematic representation of the effect of Coulomb (ionized impurity) scattering, acoustic and intervalley phonon scattering, and surface-roughness scattering, as well as temperature, on the electron mobility [34].

The first method used the current equation in the linear region of the I_D-V_D curve of the MOSFET device in order to calculate the mobility:

$$\begin{aligned} I_D &= \mu C_{ox} \frac{W}{L}(V_G - V_{th})V_D, \\ C_{ox} &= \frac{\varepsilon_{ox}}{t_{ox}}, \end{aligned} \tag{47}$$

where μ is the mobility, C_{ox} is the oxide capacitance where ε_{ox} is the permittivity of the oxide, t_{ox} is the thickness of the oxide, W is the width of the device, L is the length of the device, and V_{th} is the threshold voltage [2, 36, 37]. However, since the threshold voltage is

not a known quantity it must be extracted from the I_D-V_G curve of the device, which was done using the extrapolation in the linear region method: V_{th} is found as the gate voltage at the axis intercept (I_D=0) in the I_D-V_G curve at its maximum slope [37–39]. Once the threshold voltage is found, the mobility is calculated by solving equation (47) for the mobility [2]. In order to calculate the channel mobility, the mobility must be calculated at drain voltages that are within the linear region of the I_D-V_D curve [39]. Additionally, the effective transverse electric field for an n-type MOSFET can be found from:

$$E_{eff,y} = \frac{V_G + V_{th}}{6t_{ox}}, \tag{48}$$

where $E_{eff,y}$ is the effective transverse electric field [37, 41]. Then, in order to create the channel mobility–effective transverse electric field curve, the mobility and effective transverse electric field are calculated at various gate voltages that are larger than the threshold voltage, while keeping the drain voltage a constant value [39].

The second method used to calculate the mobility and the effective transverse electric field was to extract the mobility and the effective electric fields at the device level by:

$$\mu(x) = \frac{\langle v_{drift}(x) \rangle}{E_{eff,x}(x)}, \tag{49}$$

where $\langle v_{drift}(x) \rangle$ is the average drift velocity in the x direction, calculated by sampling the motion of the electrons in the device in the Monte Carlo simulation described in section 2.1 and $E_{eff,x}(x)$ is the effective lateral electric field in the x direction [4, 39, 40]. Both of the effective electric fields of the MOSFET device were calculated by averaging the values along the depth of the device:

$$E_{eff}(x) = \frac{\int_0^{y_{max}} E(x,y)n(x,y)dy}{\int_0^{y_{max}} n(x,y)dy}, \tag{50}$$

where $n(x, y)$ is the electron concentration in the device [40]. The average drift velocity in the x direction is also calculated using the same formula in equation (50), replacing the electric field with the drift velocity [40]. Once all of the values are obtained the mobility can then be calculated from equation (49). The channel mobility–effective transverse electric field curve is then obtained by plotting these values inside the channel region of the device. However, these mobility values are very sensitive and should be averaged over a small depth in the device and must be plotted near the middle of the channel region, away from the source and drain, in order to avoid extraneous values due to the electric-field variation near the source and drain contacts.

4.4 Mobility–Electric Field Curves

As mentioned in section 4.2, the MOSFETs that were simulated for all the various methods of modeling the surface-roughness scattering of electrons were the MOSFETs described in section 1.2 with Coulomb, acoustic, and intervalley scattering mechanisms already present. Additionally, for both MOSFET devices, the mobility and electric fields were calculated only using the first method described in section 4.3 where the mobility and electric field are both calculated from the I_D-V_D curves. The calculations of the mobility and electric field from the device level was conducted and plotted, however, due to the sensitivity of the mobility calculation using this method and its dependence on having a large number of electrons initialized in the device, the values did not approach reasonable mobility values for a MOSFET, and therefore the curves are not displayed. However, the mobility–electric field curves would have looked similar to those calculated from the current method, if the MOSFET devices had been initialized with enough electrons. Also as was done in section 4.2, for all of the mobility curves for both devices the constant specularity parameters of $p = 1$ (perfectly smooth) and $p = 0$ (perfectly rough) are displayed for reference, to compare each curve to the two extremes for the constant-specularity-parameter method [5, 20]. Also, as was mentioned for the current–voltage curves it is possible for the mobility–electric field curves to display a curves that are lower than the rough curve simulated by the constant-specularity-parameter method, due to the limitations in the roughness simulation with the constant-specularity-parameter method.

4.4.1 250-nm MOSFET Devices

For the 250-nm device, the mobility–electric field curves obtained from the constant-specularity-parameter method (as described in section 3.1) are shown in Figure 23. These curves were simulated with $p = 0.5$ (fairly rough surface), as well as the two extreme values, in order to demonstrate the range of values that are obtainable using the constant-specularity-parameter method. As can be seen from the curves, the channel mobility of the electrons greatly decreases due to the surface-roughness scattering.

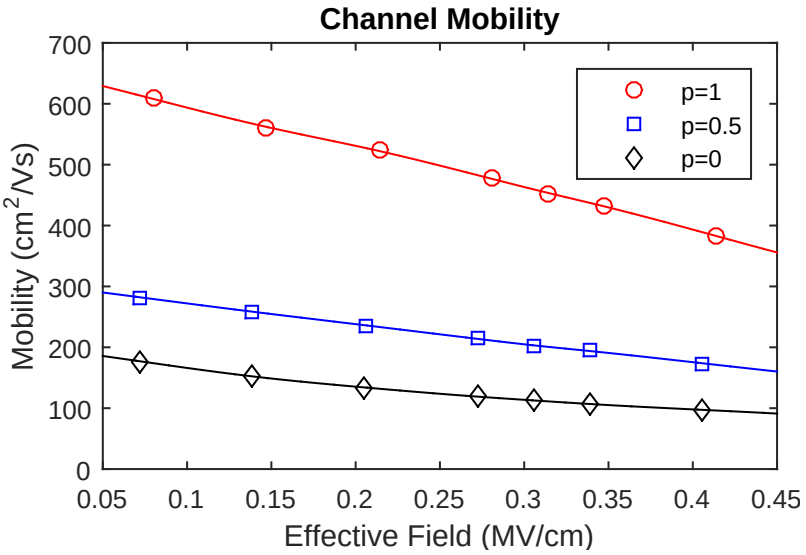

Figure 23: Mobility–electric field curves for a 250-nm MOSFET using the constant-specularity-parameter method. The red and black curves display the two extremes, perfectly smooth and, rough respectively, and the blue curve is a fairly rough MOSFET.

The channel mobility–electric field curve for the momentum-dependent specularity-parameter method with an rms roughness height of 2 Å [1] is shown in Figure 24.

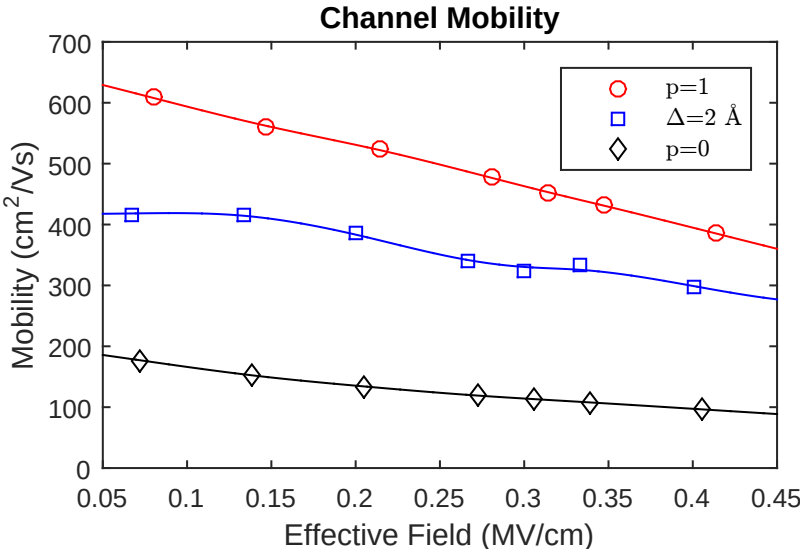

Figure 24: Mobility–electric field curve for a 250-nm MOSFET using the momentum-dependent specularity-parameter method with an rms roughness height for an unintentionally roughened MOSFET. The red and black curves display the two extremes, perfectly smooth and rough, respectively, and the blue curve displays a MOSFET with rms roughness height of 2 Å.

The channel mobility–electric field curve for the momentum-dependent specularity-parameter method using an rms roughness height of 5 Å [1, 27] is shown in Figure 25. Both of the momentum-dependent specularity-parameter curves are within the two extremes.

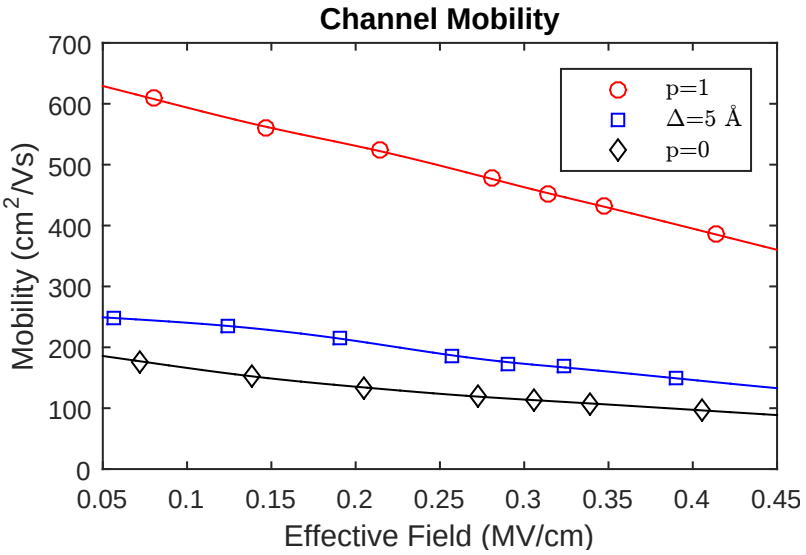

Figure 25: Mobility–electric field curve for a 250-nm MOSFET using the momentum-dependent specularity-parameter method with an rms roughness height for an intentionally roughened MOSFET. The red and black curves display the two extremes, perfectly smooth and rough, respectively, and the blue curve displays a MOSFET with rms roughness height of 5 Å.

The channel mobility–electric field curve for a real-space rough surface with a uniform electric field, as described in section 3.3 for a MOSFET with $\Delta = 2$ Å, $\xi = 35$ Å is shown in Figure 26. The curve is similar to the perfectly smooth constant-specularity-parameter curve, since the electrons scatter from the uniform electric field, instead of the rough surface.

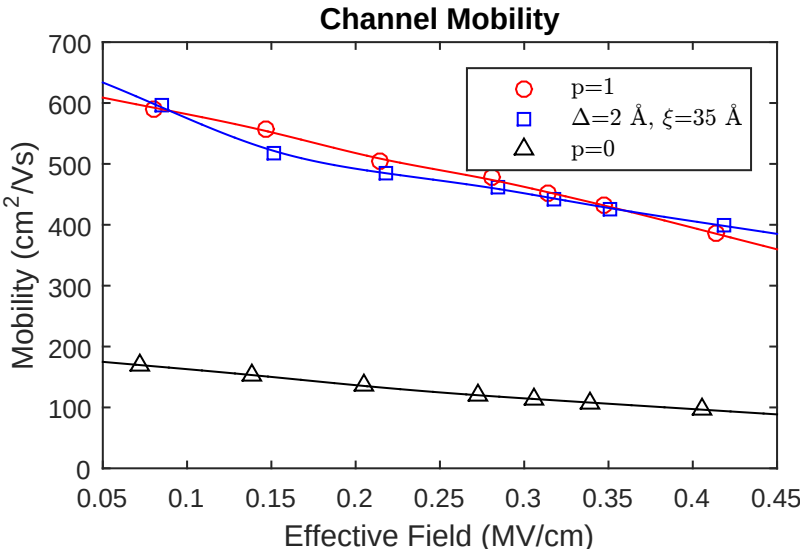

Figure 26: Mobility–electric field curve for a 250-nm MOSFET using a real-space rough-surface method with a uniform electric field, 0.5 nm mesh, $\Delta = 2$ Å, and $\xi = 35$ Å. The red and black curves display the two extremes, perfectly smooth and rough, respectively, and the blue curve displays a MOSFET with an rms roughness height of 2 Å and correlation length of 35 Å.

The channel mobility–electric field curve for the real-space roughness with a varying electric field, as described in section 3.3 for an unintentionally roughened MOSFET ($\Delta =$

2 Å, $\xi = 35$ Å) [1] is shown in Figure 27.

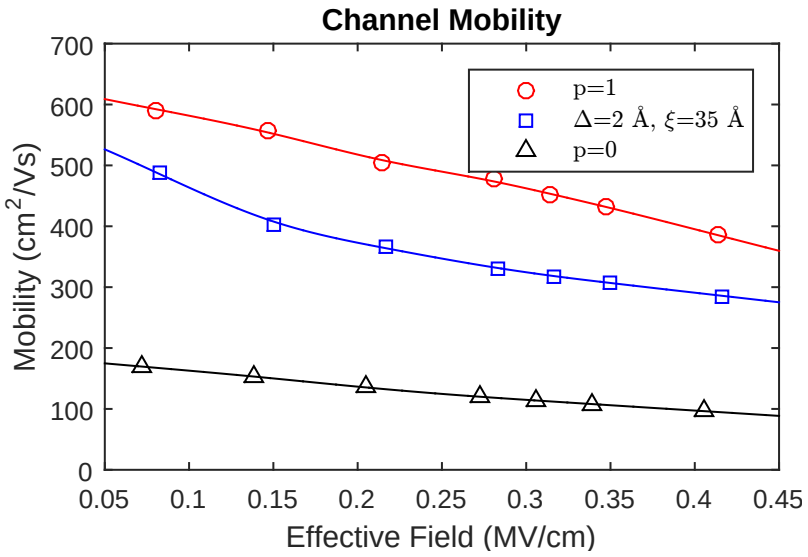

Figure 27: Mobility–electric field curves for a 250-nm MOSFET using a real-space rough-surface mehtod with a varying electric field, 0.5 nm mesh, and an rms roughness height and correlation length for an unintentionally roughened MOSFET. The red and black curves display the two extremes, perfectly smooth and rough, respectively, and the blue curves display a MOSFET with an rms roughness height of 2 Å and correlation length of 35 Å.

The channel mobility–electric field curve for the real-space roughness with a varying electric field for an intentionally roughened MOSFET ($\Delta = 3$Å, $\xi = 40$Å) [1] is shown in Figure 28. Both of the real-space roughness with a varying electric field curves are within the two extremes, displaying the method's validity.

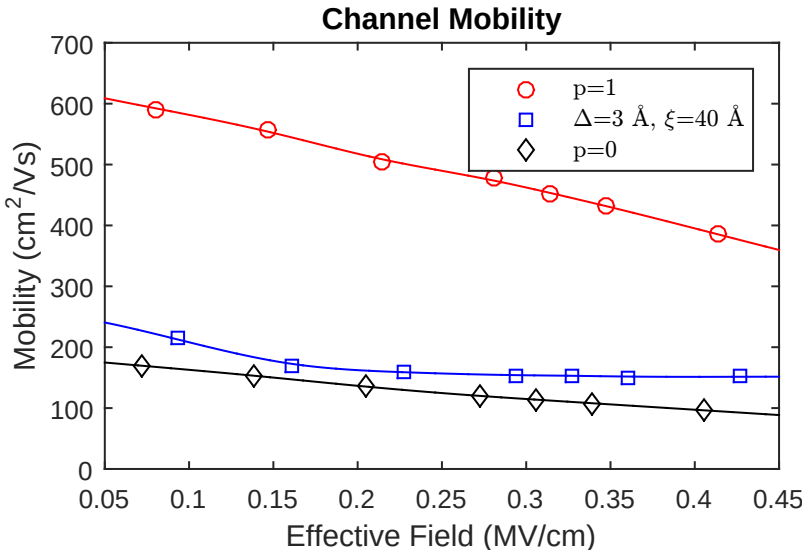

Figure 28: Mobility–electric field curves for a 250-nm MOSFET using a real-space rough-surface method with a varying electric field, 0.5 nm mesh, and an rms roughness height and correlation length for an intentionally roughened MOSFET. The red and black curves display the two extremes, perfectly smooth and rough, respectively, and the blue curves display a MOSFET with an rms roughness height of 3 Å and correlation length of 40 Å.

As was seen for the current–voltage curves, when comparing the real-space roughness curves with a varying electric field, the surface-roughness effect greatly increases even with a small change in the rms roughness height and correlation length, demonstrating that even a small amount of roughness can degrade the mobility of the device.

4.4.2 50-nm MOSFET Devices

The decrease from the 250-nm device to the 50-nm device decreases the mobility of the electrons in the device, due to the large decrease in channel length, which starts causing short channel effects. Additionally, the device width was increased in order to increase the number of electrons to have enough for calculating the mobility at the device level, however, the number of electrons was still not sufficient. For the 50-nm device the mobility–electric field curves obtained from the constant-specularity-parameter method as described in section 3.1 are shown in Figure 29. These curves were simulated with $p = 0.5$, as well as the two extreme values. As can be seen from the curves, the channel mobility of the electrons can greatly decrease due to the surface-roughness scattering.

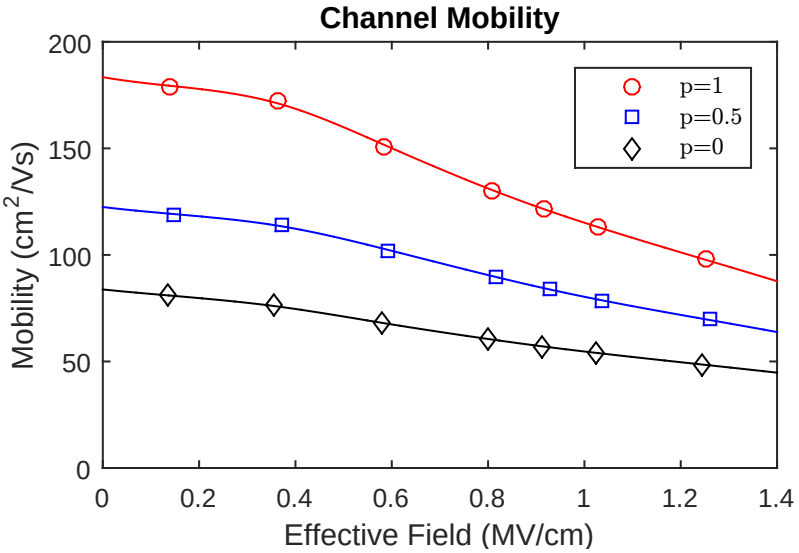

Figure 29: Mobility–electric field curves for a 50-nm MOSFET using the constant-specularity-parameter method. The red and black curves display the two extremes, perfectly smooth and rough, respectively, and the blue curve is a fairly rough MOSFET.

The channel mobility–electric field curve for the momentum-dependent specularity-parameter method with an rms roughness height of 2 Å [1] is shown in Figure 30.

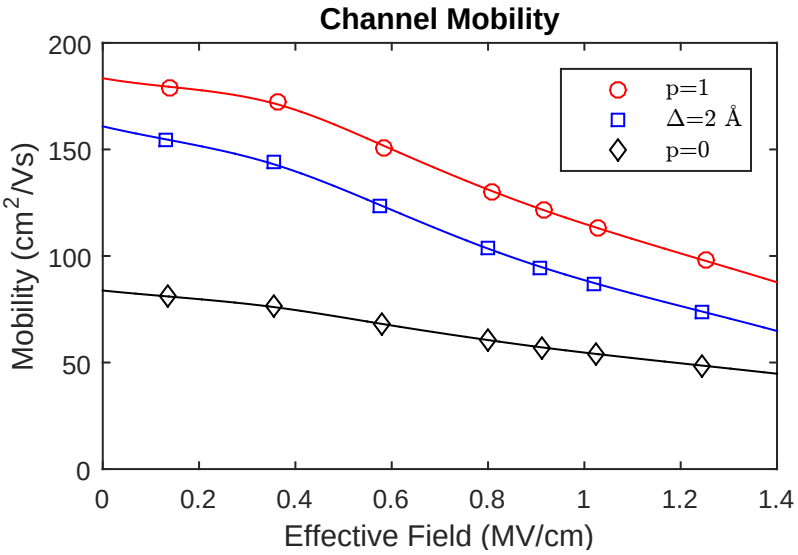

Figure 30: Mobility–electric field curves for a 50-nm MOSFET using the momentum-dependent specularity-parameter method with an rms roughness height for an unintentionally roughened MOSFET. The red and black curves display the two extremes, perfectly smooth and rough, respectively, and the blue curve displays a MOSFET with rms roughness height of 2 Å.

The channel mobility–electric field curve for the momentum-dependent specularity-parameter method using an rms roughness height of 5 Å [1, 27] is shown in Figure 31. Both of the momentum-dependent-specularity-parameter curves are within the two extremes, displaying the method's validity.

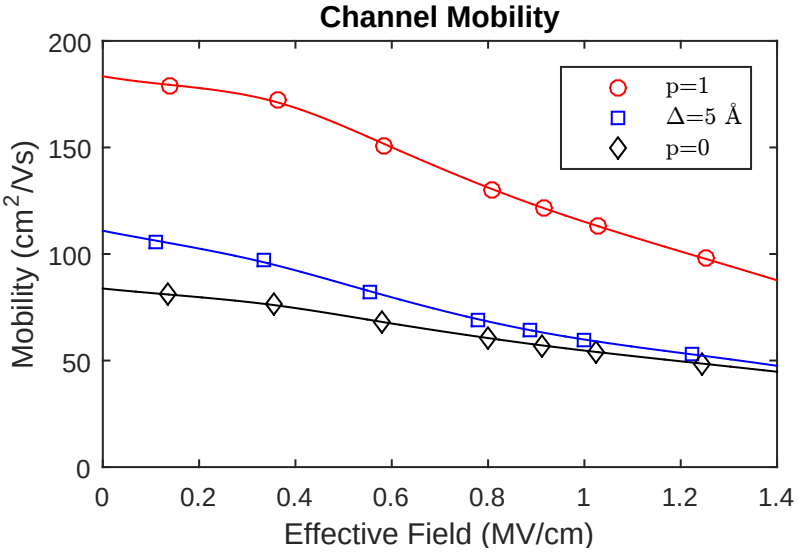

Figure 31: Mobility–electric field curves for a 50-nm MOSFET using the momentum-dependent specularity-parameter method with an rms roughness height for an intentionally roughened MOSFET. The red and black curves display the two extremes, perfectly smooth and rough, respectively, and the blue curve displays a MOSFET with rms roughness height of 5 Å.

The channel mobility–electric field curve for real-space roughness with a uniform electric field, as described in section 3.3 for a MOSFET with $\Delta = 2$ Å, $\xi = 35$ Å is shown in

Figure 32. As for the 250-nm device case, the real-space roughness with a uniform electric field curve is similar to the perfectly smooth constant-specularity-parameter curve.

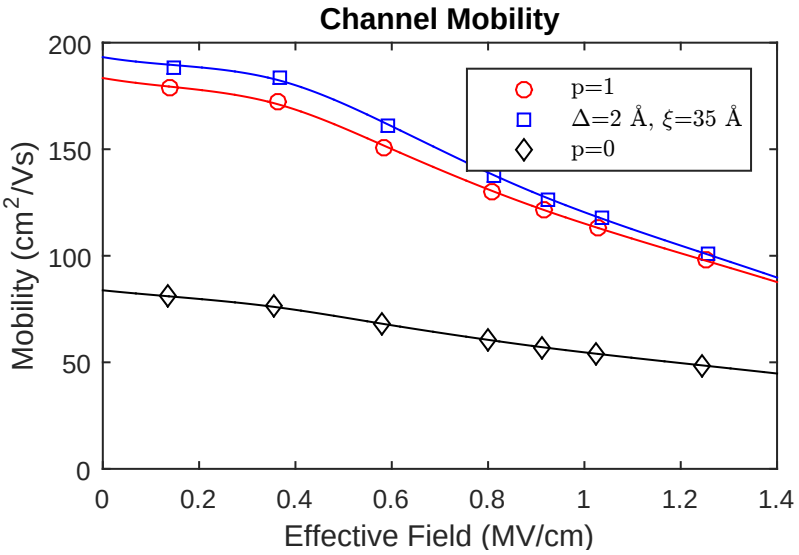

Figure 32: Mobility–electric field curve for a 50-nm MOSFET using a real-space rough-surface method with a uniform electric field, $\Delta = 2$ Å, and $\xi = 35$ Å. The red and black curves display the two extremes, perfectly smooth and rough, respectively, and the blue curve displays a MOSFET with an rms roughness height of 2 Å and correlation length of 35 Å.

The channel mobility–electric field curve for the real-space roughness with a varying electric field, as described in section 3.3 for an unintentionally roughened MOSFET ($\Delta = 2$ Å, $\xi = 35$ Å) [1] is shown in Figure 33.

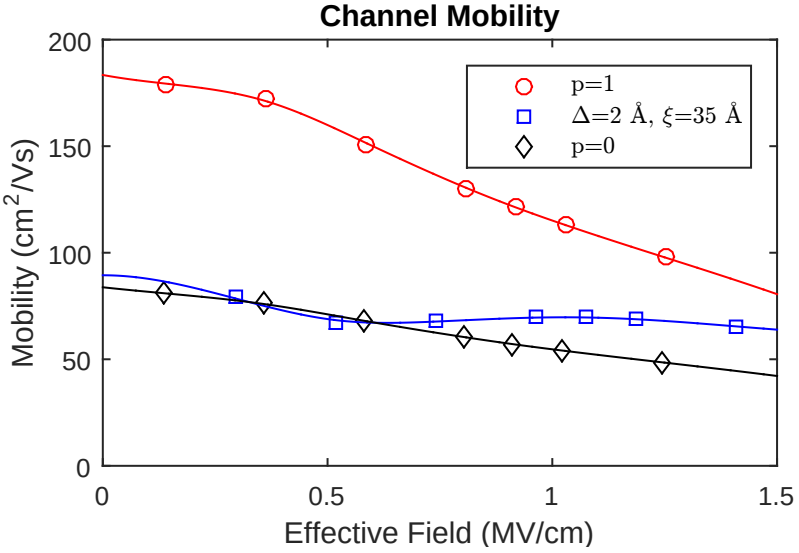

Figure 33: Mobility–electric field curves for a 50-nm MOSFET using a real-space rough-surface method with a varying electric field, and an rms roughness height and correlation length for an unintentionally roughened MOSFET. The red and black curves display the two extremes, perfectly smooth and rough, respectively, and the blue curves display a MOSFET with an rms roughness height of 2 Å and correlation length of 35 Å.

The channel mobility–electric field curve for the real-space roughness with a varying electric field for an intentionally roughened MOSFET ($\Delta = 3$ Å, $\xi = 40$ Å) [1] is shown in Figure 34. As with the current–voltage curves, both sets of the mobility–electric field curves for the 50-nm device are close to or below the perfectly rough curve from the constant-specularity-parameter method. The real-space roughness with a varying electric field curves display larger roughness for the 50-nm device because the 50-nm device allows for a larger amount of roughness along the channel of the device, due to the decrease in the mesh size from 0.5 nm to 0.2 nm from the 250-nm device to the 50-nm device. Instead of having large roughness at just the ends of the channel, the 50-nm device has finer roughness more throughout the channel of the device. The additional roughness in the channel causes more scattering of the electrons, and therefore a more realistic roughness in the device.

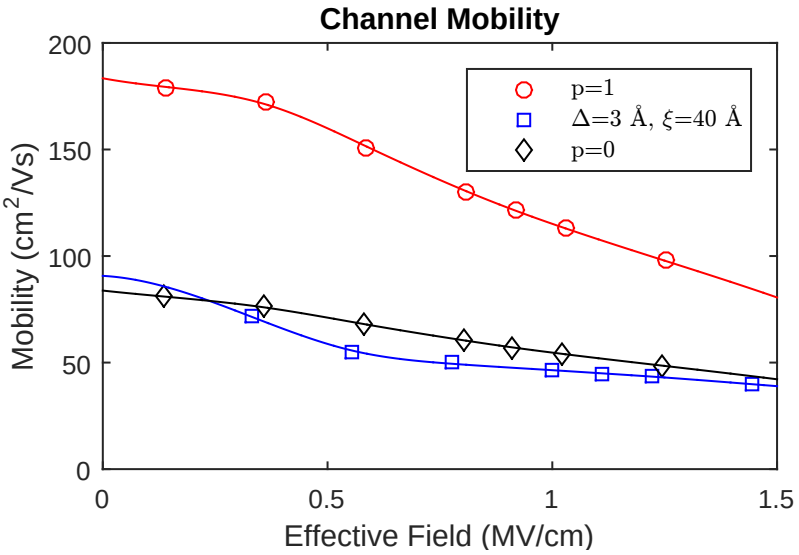

Figure 34: Mobility–electric field curves for a 50-nm MOSFET using a real-space rough-surface method with a varying electric field, and an rms roughness height and correlation length for an intentionally roughened MOSFET. The red and black curves display the two extremes, perfectly smooth and rough, respectively, and the blue curves display a MOSFET with an rms roughness height of 3 Å and correlation length of 40 Å.

5 Conclusion and Future Work

In this project, a 250-nm bulk MOSFET with a uniform mesh and a 50-nm bulk MOSFET with a non-uniform mesh were simulated with different methods for calculating surface-roughness scattering of electrons. The methods that were simulated are the constant-specularity-parameter method, momentum-dependent specularity-parameter method, real-space roughness with a uniform electric field, and real-space roughness with a varying electric field. All of the simulations use device parameters for a Si MOSFET and use ensemble Monte Carlo to solve the Boltzmann transport equation. The simulation also includes the successive over-relaxation method, used to solve the two-dimensional Poisson's equation. The specularity-parameter methods used assume an electron scatters from the surface of the device instead of the electric field. For the real-space rough-surface method, the electron has Coulomb interaction with a spatially varying electric field. All of the methods were simulated on both MOSFET devices, and the current–voltage and mobility–electric field curves were plotted.

The constant-specularity-parameter curves were simulated for three parameters: perfectly smooth (p=1), fairly rough (p=0.5), and perfectly rough (p=0). The momentum-dependent specularity parameter was used with two different rms roughness heights and was shown to approximate a fairly large range of roughness, similar to the constant-specularity-parameter method. The real-space rough surface with a uniform electric field was simulated with both unintentionally roughened and intentionally roughened rms roughness heights and correlation lengths. Both sets of curves displayed features similar to those of a perfectly smooth interface, since the electrons do not observe the roughness because the field is kept uniform. Lastly, the real-space roughness with a varying electric field was also simulated with both unintentionally roughened and intentionally roughened rms and correlation lengths. The 250-nm MOSFET was simulated with a uniform mesh of 0.5 nm for the real-space rough surface and therefore was not able to have a fine rough surface. Instead, the rough surface was fairly flat in the middle of the channel, causing the electrons to not scatter from surface-roughness in large areas of the long channel of the device. The 50-nm MOSFET was simulated with a non-uniform mesh, with a mesh size of 0.2 nm at the interface of the device, and therefore was able to have a much finer rough surface throughout a larger area in the channel than the 250-nm device. The 50-nm devices displayed a larger amount of degradation due to the roughness scattering than the 250-nm device. For instance, using the real-space roughness method both the current–voltage and mobility–electric field curves were more degraded than the perfectly rough (p=0) constant-specularity-parameter method. The 250-nm device would display degradation greater than obtained for the perfectly rough (p=0) constant-specularity-parameter method, as well. However, due to the larger mesh size from using a uniform mesh, the data displayed for the 250-nm device for the real-space roughness method are

not as accurate as for the 50-nm device.

Future work includes simulations with larger electron ensembles, which would enable more accurate calculations of the position-dependent channel mobility. Additionally, this project could be expanded to display the surface-roughness scattering non-planar devices, such as the three-dimensional FinFET. Lastly, the simulations could be compared to experimentally derived data for the operation of MOSFET devices with the same device parameters, rms roughness heights, and correlation lengths to determine the real-world validity of the models used in this project.

6 References

[1] S.M. Goodnick et al.,"Surface roughness at the Si(100)- SiO_2 interface", *Physical Review B*, vol. 32, no. 12, pp. 8171-8186, 1985.

[2] M. Lundstrom, *Fundamentals of Carrier Transport*. Cambridge, U.K.: Cambridge University Press, 2000.

[3] T. Ando, A.B. Fowler, and F. Stern,"Electronic properties of two-dimensional systems", *Reviews of Modern Physics*, vol. 54, no. 2, pp. 437-672, 1982.

[4] D. Vasileska, S.M. Goodnick, and G. Klimeck, *Computational Electronics: Semiclassical and Quantum Device Modeling and Simulation*. Boca Raton: CRC Press, 2010.

[5] J.M. Ziman, *Electrons and Phonons: The Theory of Transport Phenomena in Solids*. Oxford: Clarendon Press, 1960.

[6] D. Vasileska and S.M. Goodnick, *Computational Electronics*. [San Rafael, Calif.]: Morgan & Claypool Publishers, 2006.

[7] M. Shin, M. Jang, and S. Lee, "Quantum mechanical simulation of charge distribution in Schottky MOSFETs", *Journal of the Korean Physical Society*, vol. 45, pp. S547-S550, 2004.

[8] X. Guo, "Algebraic multigrid Poisson equation solver", M.S. thesis, Arizona State University, 2015.

[9] S. Selberherr, *Analysis and Simulation of Semiconductor Devices*. New York: Springer-Verlag Wien, 1984.

[10] C. Jacoboni and P. Lugli, *The Monte Carlo Method for Semiconductor Device Simulation*. New York: Springer-Verlag Wien, 1989.

[11] S. Milicic,"Three dimensional modeling of silicon quantum dots", M.S. thesis, Arizona State University, 2000.

[12] C. Galup-Montoro and M. Schneider, *MOSFET Modeling for Circuit Analysis and Design*. Singapore: World Scientific, 2007.

[13] R. J. Gonsalves. (2011). *Poisson's equation and relaxation methods* [Online]. Available: http://www.physics.buffalo.edu/phy410-505/2011/topic3/app1/index.html

[14] Y. Shi, "Ensemble Monte Carlo simulation of the 4.8m deep well quantum cascade lasers", M.S. thesis, University of Wisconsin-Madison, 2010.

[15] C. Jacoboni and L. Reggiani, "The Monte Carlo method for the solution of charge transport in semiconductors with applications to covalent materials", *Reviews of Modern Physics*, vol. 55, no. 3, pp. 645-705, 1983.

[16] K. Tomizawa, *Numerical Simulation of Submicron Semiconductor Devices*. Boston: Artech House, 1993.

[17] I. Knezevic, D.Z. Vasileska and D.K. Ferry, "Impact of strong quantum confinement on the performance of a highly asymmetric device structure: Monte Carlo particle-based simulation of a focused-ion-beam MOSFET", 2002. *IEEE Trans. Electron Devices*, vol. 49, no. 6, pp. 1019-1026,

[18] J.A. Ogilvy, *Theory of Wave Scattering From Random Rough Surfaces*. Bristol, England: A. Hilger, 1991.

[19] X. Wang and B. Huang, "CORRIGENDUM: Computational Study of In-Plane Phonon Transport in Si Thin Films", *Scientific Reports*, vol. 5, p. 7604, 2015.

[20] S.B. Soffer,"Statistical Model for the Size Effect in Electrical Conduction", *J. Appl. Phys.*, vol. 38, no. 4, p. 1710, 1967.

[21] O.M. Bulashenko, O.V. Kochelap, and V.A. Kochelap,"Size effect on current fluctuations in thin metal films: Monte Carlo approach", *Physical Review B*, vol. 45, no. 24, pp. 14308-14314, 1992.

[22] M.F. Modest, *Radiative Heat Transfer*. Amsterdam: Academic Press, 2003.

[23] L. Devroye, *Non-Uniform Random Variate Generation*. New York: Springer-Verlag, 1986.

[24] D. Lacroix, K. Joulain, and D. Lemonnier, "Monte Carlo transient phonon transport in silicon and germanium at nanoscales", *Physical Review B*, vol. 72, no. 6, 2005.

[25] Z. Aksamija and I. Knezevic,"Thermal conductivity of $Si_{1-x}Ge_x/Si_{1-y}Ge_y$ superlattices: Competition between interfacial and internal scattering", *Physical Review B*, vol. 88, no. 15, 2013.

[26] L.N. Maurer et al.,"Universal features of phonon transport in nanowires with correlated surface roughness", *Applied Physics Letters*, vol. 106, no. 13, p. 133108, 2015.

[27] E.B. Ramayya et al.,"Thermoelectric properties of ultrathin silicon nanowires", *Physical Review B*, vol. 86, no. 11, 2012.

[28] R.L. Burden, D.J. Faires, and A.M. Burden, *Numerical Analysis*. 10th ed. Boston: Cengage Learning, 2016.

[29] J. Jong-Wu,"Simulation of rough surfaces with FFT", *Tribology International*, vol. 33, no. 1, pp. 47-58, 2000.

[30] D. Han, H. Han and S. Ohmi, "Impact of Si surface roughness on MOSFET characteristics with ultrathin HfON gate insulator formed by ECR plasma sputtering", *IEICE Electron. Express*, vol. 10, no. 18, pp. 20130651-20130651, 2013.

[31] W. Chen, *The Circuits and Filters Handbook*. 2nd ed. Boca Raton, FL: CRC Press, 2003.

[32] The MathWorks, Inc. (2015). *Least-squares fitting -MATLAB & Simulink* [Online]. Available: http://www.mathworks.com/help/curvefit/least-squares-fitting.html

[33] G. Ledder, *Mathematics for the Life Sciences:Calculus, Modeling, Probability and Dynamical Systems*. New York: Springer, 2013.

[34] S. Takagi et al., "On the universality of inversion layer mobility in Si MOSFET's: Part I-effects of substrate impurity concentration", *IEEE Trans. Electron Devices*, vol. 41, no. 12, pp. 2357-2362, 1994.

[35] S. Takagi et al., "On the universality of inversion layer mobility in Si MOSFET's: Part II-effects of surface orientation", *IEEE Trans. Electron Devices*, vol. 41, no. 12, pp. 2363-2368, 1994.

[36] D.S. Jeon and D.E. Burk, "MOSFET electron inversion layer mobilities-a physically based semi-empirical model for a wide temperature range", *IEEE Trans. Electron Devices*, vol. 36, no. 8, pp. 1456-1463, 1989.

[37] K.J. Yang et al., "Electron mobility in MOSFETs with ultrathin RTCVD silicon nitride/oxynitride stacked gate dielectrics", *Solid-State Electronics*, vol. 47, no. 1, pp. 149-153, 2003.

[38] A. Ortiz-Conde et al., "A review of recent MOSFET threshold voltage extraction methods", *Microelectronics Reliability*, vol. 42, no. 4-5, pp. 583-596, 2002.

[39] K. Ryu et al., "Direct extraction of mobility in pentacene OFETs using C-V and I-V measurements", *IEEE Electron Device Lett.*, vol. 26, no. 10, pp. 716-718, 2005.

[40] I. Knezevic et al., "Low-field mobility and quantum effects in asymmetric silicon-based field-effect devices", *Journal of Computational Electronics*, vol. 1, no. 12, pp. 273-277, 2002.

[41] D.K. Schroder, *Semiconductor Material and Device Characterization*. 3rd ed. New York [etc.]: John Wiley & Sons, 2006.